Enrichment of the Galactic disc with neutron capture elements: Sr

T. Mishenina, M. Pignatari, T. Gorbaneva, S. Bisterzo, C. Travaglio, F. K. Thielemann, C. Soubiran

Monthly Notices
of the
ROYAL ASTRONOMICAL SOCIETY

MNRAS **484,** 3846–3864 (2019) doi:10.1093/mnras/stz178

Enrichment of the Galactic disc with neutron capture elements: Sr

T. Mishenina,[1]★ M. Pignatari,[2,3]★† T. Gorbaneva,[1] S. Bisterzo,[4,5]† C. Travaglio,[4,5]† F.-K. Thielemann[6] and C. Soubiran[7]

[1]*Astronomical Observatory, Odessa National University and Isaac Newton Institute of Chile, Odessa branch, Shevchenko Park, 65014 Odessa, Ukraine*
[2]*E.A. Milne Centre for Astrophysics, Dept of Physics & Mathematics, University of Hull, Hull HU6 7RX*
[3]*Konkoly Thege Miklos ut 15-17, H-1121 Budapest, Hungary*
[4]*INFN, Istituto Nazionale Fisica Nucleare, Via Pietro Giuria 1, 10125 Turin, Italy*
[5]*B2FH Association, Turin, Italy*
[6]*Department of Physics, University of Basel, Klingelbergstrabe 82, 4056 Basel, Switzerland*
[7]*Laboratoire d'Astrophysique de Bordeaux, Univ. Bordeaux–CNRS, B18N, allée Geoffroy Saint-Hilaire, 33615 Pessac, France*

Accepted 2019 January 15. Received 2019 January 15; in original form 2018 May 15

ABSTRACT

The enrichment history of heavy neutron-capture elements in the Milky Way disc provides fundamental information about the chemical evolution of our Galaxy and the stellar sources that made those elements. In this work we give new observational data for Sr, the element at the first neutron-shell closure beyond iron, $N = 50$, based on the analysis of high-resolution spectra of 276 Galactic disc stars. The Sr abundance was derived by comparing the observed and synthetic spectra in the region of the Sr I 4607 Å line, making use of the local thermodynamic equilibrium (LTE) approximation. Non-local thermodynamic equilibrium (NLTE) corrections lead to an increase in the abundance estimates obtained under LTE, but for this line they are minor near solar metallicity. The average correction that we find is 0.151 dex. The star that is mostly affected is HD 6582, with a 0.244 dex correction. The behaviour of the Sr abundance as a function of metallicity is discussed within a stellar nucleosynthesis context, in comparison with the abundance of the heavy neutron-capture elements Ba ($Z = 56$) and Eu ($Z = 63$). Comparison of the observational data with current Galactic chemical evolution (GCE) models confirms that *s*-process contributions from asymptotic giant branch stars and massive stars are the main sources of Sr in the Galactic disc and the Sun, while different nucleosynthesis sources can explain the high [Sr/Ba] and [Sr/Eu] ratios observed in the early Galaxy.

Key words: stars: abundances – stars: late-type – Galaxy: disc – Galaxy: evolution.

1 INTRODUCTION

The study of the chemical enrichment history of stars in our Galaxy allows us to benchmark our understanding of its formation and evolution and also stellar evolution and nucleosynthesis. Across the evolution of the Galaxy, elements have been made by different generations of stars, building up the abundance pattern also observed today in the Sun (e.g. Matteucci & Greggio 1986; Timmes, Woosley & Weaver 1995; Goswami & Prantzos 2000; Gibson et al. 2003; Kobayashi, Karakas & Umeda 2011). Despite their low abundance relative to other metals lighter than iron, heavy elements provide powerful constraints for chemical evolution and other nuclear astrophysics disciplines. According to the established scenario of nucleosynthesis of heavy elements in stars, about half of the abundances beyond iron are due to the slow neutron capture process or *s*-process (e.g. Käppeler et al. 2011 and references therein) and half to the rapid neutron capture process or *r*-process (e.g. Thielemann et al. 2017; Cowan et al. 2019 and references therein). However, in the last 20 years a growing number of theoretical and observational works provide evidence of the existence of other nucleosynthesis processes feeding the production of heavy elements, at least up to the first neutron-magic peak beyond Fe, where elements Sr, Y and Zr are located. Different types of neutrino-driven wind components from forming proto-neutron stars in core-collapse supernovae (CCSNe) have been shown potentially to contribute to the production of these elements, at least in the early Galaxy (e.g. Fröhlich et al. 2006; Farouqi et al. 2009; Roberts, Woosley & Hoffman 2010; Arcones & Montes 2011; Wanajo, Janka & Kubono 2011b; Martínez-Pinedo, Fischer & Huther 2014; Curtis et al. 2019). Wanajo, Janka & Müller (2011a) also discussed nucleosynthesis production of these elements in electron-capture supernovae.

* E-mail: tmishenina@ukr.net (TM); mpignatari@gmail.com (MP)
† The NuGrid collaboration, http://www.nugridstars.org

A number of nucleosynthesis processes needed at low metallicity have also been discussed by Hansen, Montes & Arcones (2014), utilizing the approach by Qian & Wasserburg (2001). These authors considered neutrino-driven winds in CCSNe as a source of Sr. More recent analyses of production of elements at the Sr peak in metal-poor stars are provided by Hansen et al. (2018) and Spite et al. (2018).

In this context, a clear understanding of the production of elements in the Sr–Y–Zr region becomes more complicated compared with the established two-component scenario, where only the *s*-process and the *r*-process are relevant. Many processes need to be taken into account to explain the observed abundances and their relative relevance may change across the history of the Galaxy. In the Galactic halo, the role of *s*-process production from asymptotic giant branch (AGB) stars in Galactic chemical evolution (GCE) is minor, even for elements that are typically classified as *s*-process elements by looking at the abundance distribution in the Solar system (e.g. Travaglio et al. 2004). Recent GCE simulations by Bisterzo et al. (2014) assign to Sr an *s*-process contribution from AGB stars of 68.9 $\pm$ 5.9 per cent, but that contribution is not significant for Sr observed in metal-poor stars. On the other hand, the *s*-process in fast rotating metal poor stars could provide a significant contribution to the Sr production observed in Galactic halo stars (Pignatari et al. 2008; Frischknecht et al. 2016) and could be marginal for the Sr abundance in the Galactic disc. A study of the Sr/Ba ratio in four halo stars (Spite et al. 2014) has shown that the abundance pattern of *s*-process elements is strikingly similar to theoretical estimates of the *s*-process. The contribution to the *s*-process from rapidly rotating stars (Choplin et al. 2017; Meynet & Maeder 2017; Nishimura et al. 2017) as the missing component responsible for the relative distribution of light (Sr) and heavy (Ba) neutron-capture elements has been studied by adopting a stochastic chemical evolution model (Cescutti et al. 2015b).

Travaglio et al. (2004) found that, in solar abundances, there is a component missing between Sr and Xe, not explained by the traditional *s*- and *r*-process scenario. They called that component the lighter element primary process (LEPP) and associated it with the Sr-rich signature observed in a large fraction of metal-poor stars. This result is still controversial (see e.g. Honda et al. 2004, 2007; Montes et al. 2007; Cristallo et al. 2015; Trippella et al. 2016). The results of Travaglio et al. (2004) did not take into account the complete zoo of processes possibly feeding at least the Sr–Y–Zr peak, and it is plausible that some of them are relevant for GCE. Sr is made through the weak *s*-process in massive stars (e.g. Raiteri et al.1991a,b; The, El Eid & Meyer 2007; Pignatari et al. 2010, 2016b) and in massive AGB stars (>4 $M_{\odot}$) (e.g. Karakas & Lattanzio 2014; Cristallo et al. 2015; Pignatari et al. 2016a). Travaglio et al. (2004) estimated the contribution from the weak *s*-process to be 9 per cent of the solar Sr. The contribution from massive AGB stars changes between 9 per cent (Travaglio et al. 2004) and 1.35 per cent (Bisterzo et al. 2014). There is not a clear estimate of the errors associated with these contributions, where both nuclear and stellar model uncertainties are taken into account consistently (e.g. Pignatari et al. 2016a). The *r*-process, together with all of these nucleosynthesis processes, made the remaining fraction of Sr that was not created by the *s*- process. However, the origin of *r*-process elements with $A > 56$ also remains controversial. At least four sources have been proposed, namely (1) neutrino-induced winds from supernovae (Woosley et al. 1994; Takahashi, Witti & Janka 1994), (2) neutron-rich matter ejected from coalescencing neutron stars (Freiburghaus, Rosswog & Thielemann 1999; Thielemann et al. 2017, see further references in the latter review), (3) winds from black hole–neutron star mergers (Surman et al. 2008) and (4) polar jet ejecta from magneto-rotational supernovae (Winteler et al. 2012; Nishimura, Takiwaki & Thielemann 2015; Nishimura et al. 2017).

In recent years, the intermediate-neutron capture process or *i*-process (Cowan & Rose 1977) has been shown to be active since the first stages of the evolution of the Galaxy, possibly explaining the anomalous abundance patterns observed in old metal-poor stars (e.g. Dardelet et al. 2014; Hampel et al. 2016; Roederer et al. 2016; Clarkson, Herwig & Pignatari 2018), younger objects in the Galactic disc and open clusters (Herwig et al. 2011; Mishenina et al. 2015; D'Orazi, De Silva & Melo 2017) and presolar grains (Fujiya et al. 2013; Liu et al. 2014).

Also, alternative sources have been introduced in several articles (Travaglio et al. 2004; Qian & Wasserburg 2008). For example, the role of neutron star mergers in the chemical evolution of the Galactic halo and the *r*-process production of Sr, Zr and Ba – complemented by *s*-process production from spin stars – was presented in Cescutti et al. (2015a). Both neutron star mergers and supernova scenarios might have contributed to producing Eu, and observations at low metallicity allow us to identify two components of *r*-process nucleosynthesis (e.g. Wehmeyer, Pignatari & Thielemann 2015). Indeed, theoretical *r*-process estimates can be tested directly with Galactic archaeology, by looking at the composition of stars formed with insufficiently mixed matter and enriched with heavy elements resulting from one or few early *r*-process events (e.g. Aoki et al. 2007; Sneden, Cowan & Gallino 2008; Roederer et al. 2010).

The Sr abundance was studied in 156 stars of the Galactic disc in a recent article by Battistini & Bensby (2016). The authors concluded that the *s*-process is responsible for the main contribution to the enrichment of Sr, with an additional contribution from a non-classical *r*-process at low metallicities. In the thin disc, the trends of [El/Fe] versus [Fe/H] are flatter, which is due to the fact that the main production from the *s*-process is balanced by Fe production from type Ia supernovae. With metallicities in the range $-1 <$ [Fe/H] < 0.3 dex, the contributions to neutron capture elements by all mentioned processes are different and change in the course of the Galaxy's evolution. In previous studies, we have determined the abundances of a number of neutron-capture elements for more than 250 stars (Mishenina et al. 2013). Here we extend our study with information on Sr and provide a comparative analysis of the abundances of elements that in the Galactic disc are made mostly by *s*-process (Sr and Y at the neutron shell closure $N = 50$ and Ba and La at $N = 82$) elements in relation to europium (Eu), produced by the *r*-process.

This article is organized as follow. The observations and selection of stars plus the definitions of the main stellar parameters are described in Section 2. The abundance determinations and the error analysis are presented in Section 3. The results and comparison with other data, as well as the application of the results to the theory of nucleosynthesis and the chemical evolution of the Galaxy, are reported in Section 4. Conclusions are drawn in Section 5.

2 OBSERVATIONS AND ATMOSPHERIC PARAMETERS

Most observations used here were previously analysed in our article on *n*-capture elements (Mishenina et al. 2013). The spectra were obtained using the 1.93-m telescope at Observatoire de Haute-Provence (OHP, France) equipped with the echelle type spectrographs ELODIE (R = 42000) for the wavelength range

4400–6800 Å and a signal-to-noise ratio (S/N) of more than 100. Our starting sample includes 276 stars, as in Mishenina et al. (2013). Also, for those stars we have searched for additional spectra in the OHP spectroscopic archive (Moultaka et al. 2004) from the SOPHIE spectrograph, which covers a similar wavelength range at a resolution of $R = 75000$. The primary processing of spectra was carried out immediately during observations (Katz et al. 1998). Further spectral processing, such as continuum placement, line depth and equivalent width (EW) measurements, etc., was conducted using the DECH20 software package by Galazutdinov (1992).

This article belongs to a set of studies of abundances in stars in the Galactic disc (Mishenina et al. 2004, 2008, 2013). We use the same stellar parameters derived for stars in our sample. To estimate the effective temperatures $T_{\rm eff}$, we used one and the same approach for 267 dwarfs in our sample; in so doing, for better control, we have applied far-wing fitting of the Hα line profiles for nine stars with metallicities below –0.6 dex. This turned out to be more suitable, since the far wings of Hα are independent of the gravity, metallicity and convection of the atmosphere model (Gratton, Carretta & Castelli 1996), and also avoided uncertainties in the calibrations, which were constructed in the range $-0.5 <$ [Fe/H] $< +0.5$ and used by us for a large fraction of dwarfs. Effective temperatures $T_{\rm eff}$ were determined by the calibration of line-depth ratios for spectral line pairs with significantly different low-level excitation potential, applying the technique introduced and developed by Kovtyukh et al. (2003). The mean random error of each single calibration was 60–70 K (it ranged from 40–45 K to 90–95 K for the most and least accurate calibrations, respectively). The usage of about 70–100 calibrations enabled us to reduce the uncertainty down to 5–7 K (for spectra with S/N ratio of 100–150). It has been shown that 105 calibrations are essentially independent of micro-turbulence, departures from local thermodynamic equilibrium (LTE), elemental abundances, rotational parameters or any other individual stellar properties. The estimated accuracy of the method varied within the range from 5–45 K for dwarfs with [Fe/H] ≥ -0.5. For most metal-poor stars of the sample, $T_{\rm eff}$ was estimated by far-wing fitting of the Hα line profiles (Mishenina & Kovtyukh 2001). We have proved in Mishenina et al. (2004) that the temperature scales adopted in Mishenina & Kovtyukh (2001) and Kovtyukh et al. (2003) are consistent.

Surface gravities log g were computed using the ionization balance, implying that the iron abundances obtained from neutral iron Fe I and ionized iron Fe II lines were similar. The two most commonly used techniques for surface gravity determination are the ionization balance of neutral and ionized species and the fundamental relation expressing the gravity as a function of the mass, temperature and bolometric absolute magnitude deduced from the parallax. A detailed study of surface gravities derived by different methods was performed by Allende Prieto et al. (1999), who reported that astrometric and spectroscopic (iron ionization balance) gravities were in good agreement within the metallicity range $-1.0 <$ [Fe/H] $< +0.3$. In our earlier article (Mishenina et al. 2004), we compared the adapted surface gravities with those determined astrometrically by Allende Prieto et al. (1999); the resulting mean difference and standard deviation were –0.01 and 0.15, respectively, for 39 common stars. This is consistent with an accuracy of 0.1 dex in our spectroscopic gravity determinations. Moreover, in each of our studies, we have been analysing the correlation between our estimates of chemical abundances and stellar parameters to justify the correctness of the latter.

The adopted value of the metallicity [Fe/H] was calculated using the iron abundance obtained from the Fe I lines. As is known (e.g. Thévenin & Idiart 1999; Shchukina & Trujillo Bueno 2001; Mashonkina et al. 2011; Bergemann et al. 2012), the lines of neutral iron are influenced by deviations from the LTE in solar and stellar spectra and hence these deviations also affect the iron abundances determined from those lines. However, within the temperature and metallicity ranges of our target stars, non-local thermodynamic equilibrium (NLTE) corrections do not exceed 0.1 dex (see e.g. Mashonkina et al. 2011).

The microturbulent velocity $V_{\rm t}$ was derived considering that the iron abundance obtained from a given Fe I line is not correlated with the equivalent width (EW) of that line.

The parameter values obtained and their comparison with the results of other authors are reported in Mishenina et al. (2004, 2008, 2013). The accuracy of our parameter determination is estimated to be $\Delta T_{\rm eff} = \pm 100$ K, $\Delta \log g = \pm 0.2$ dex, $\Delta V_{\rm t} = \pm 0.2$–km s^{-1}, Δ[Fe/H] $= \pm 0.1$ dex. In this study, we have compared the adopted parameters with those obtained recently by Battistini & Bensby (2016) and Delgado Mena et al. (2017), who reported Sr abundances estimated in the LTE approximation using the same Sr I line as in this study. In particular, our goal was to assess the $T_{\rm eff}$ scale in our study, which is essential for Sr abundance determinations. The results of the comparison for individual stars are given in Table 1, while Table 2 presents the mean differences and errors (standard deviations) in the parameter values for the common set of target stars in various articles. In these tables, we have also provided the results of the comparison of our Sr data with those obtained earlier (Reddy et al. 2003; Mashonkina & Gehren 2001; Brewer & Carney 2006); note that the Sr II line was used in the last two studies.

We find a concordance between our data and those of Battistini & Bensby (2016) within the stated error definitions, except for $T_{\rm eff}$ for the stars HD 135204, 152391, 157089, 159482, 199960, 201891 and log g for the star HD 135204. At that the average difference values of $<\Delta T_{\rm eff}>$, $<\Delta \log g>$ and $<\Delta$ [Fe/H] $>$ are equal to -4 ± 116, -0.13 ± 0.15 and -0.03 ± 0.07, respectively. Matching our results with those of Delgado Mena et al. (2017), we obtained average values $<\Delta T_{\rm eff}> = 27 \pm 36$, $<\Delta \log g> = -0.08 \pm 0.13$ and $<\Delta$ [Fe/H] $> = -0.01 \pm 0.03$, which show good agreement between themselves.

Earlier, we carried out kinematic classification of thin- and thick-disc stars, as well as Hercules stream stars (Mishenina et al. 2004), based on *Hipparcos* (ESA 1997) parallaxes and proper motions combined with radial velocities measured by cross-correlation of the ELODIE spectra (with an accuracy better than 100 m s^{-1}). We have not updated our classification with respect to the latest astrometric data from the *Gaia* Data Release 2 (Gaia Collaboration et al. 2018), due to the fact that either many stars of our sample are too bright to be measured by *Gaia* or the relevant astrometric errors are equivalent to those of the *Hipparcos* observations. The classification is based on the (U, V, W) velocities with respect to the Sun, with typical errors of 1 km s^{-1}. Having assumed that our sample represents three populations of stars in the solar vicinity, such as those of the thin and thick disc, as well as the Hercules stream group, we have computed the probability of each star's membership in either of these populations. In these computations, we have adapted the velocity ellipsoids determined by Soubiran, Bienaymé & Siebert (2003). A star is considered to belong to a certain population if the probability was higher than 70 per cent. Application of this criterion implies that there are a number of stars with intermediate kinematics, which cannot be classified.

Table 1. Parameters of our target stars and comparison with Battistini & Bensby (2016); Delgado Mena et al. (2017); Mashonkina & Gehren (2001); Reddy et al. (2003); Brewer & Carney (2006) for common stars.

HD	$T_{\rm eff}$, K	log g	[Fe/H]	HD	$T_{\rm eff}$, K	log g	[Fe/H]	$\Delta T_{\rm eff}$, K	Δ log g	Δ [Fe/H]
	our				Battistini & Bensby (2016)					
8648	5841	4.3	0.22	8648	5790	4.2	0.12	51	0.1	0.1
22879	5972	4.5	−0.77	22879	5825	4.42	−0.91	145	0.08	0.1
30495	5790	4.5	0.02	30495	5820	4.4	−0.05	−30	0.1	0.07
64606	5188	4.4	−0.91	64606	5250	4.2	−0.91	−62	0.2	0
64815	5763	3.9	−0.35	64815	5864	4	−0.33	−101	−0.1	−0.02
135204	5200	4.4	−0.19	135204	5413	4	−0.16	−213	0.4	−0.03
152391	5322	4.5	−0.08	152391	5495	4.3	−0.08	−173	0.2	0
157089	5915	4.3	−0.5	157089	5785	4	−0.56	130	0.3	−0.06
159482	5760	4.3	−0.81	159482	5620	4.1	−0.89	140	0.2	0.08
159909	5671	4.3	0.03	159909	5749	4.1	0.06	−78	0.2	−0.03
165401	5794	4.5	−0.4	165401	5877	4.3	−0.36	−83	0.2	−0.04
178428	5656	4.2	0.15	178428	5695	4.4	0.14	−39	−0.2	0.01
187897	5944	4.5	0.12	187897	5887	4.3	0.08	57	0.2	0.04
190360	5572	4.5	0.26	190360	5606	4.4	0.12	−34	0.1	0.14
199960	6023	4.4	0.33	199960	5878	4.2	0.23	145	0.2	0.1
201891	5973	4.3	−1.08	201891	5850	4.4	−0.96	123	−0.1	−0.12
217014	5858	4.4	0.24	217014	5763	4.3	0.17	95	0.1	0.07
	our				Delgado Mena et al. (2017)					
4307	5889	4.0	−0.18	4307	5840	4.13	−0.21	49	−0.13	0.03
14374	5449	4.3	−0.09	14374	5375	4.42	−0.07	74	−0.12	−0.03
22049	5084	4.4	−0.15	22049	5049	4.45	−0.15	35	−0.05	0.0
22879	5972	4.5	−0.77	22879	5949	4.68	−0.79	23	−0.18	0.02
38858	5776	4.3	−0.23	38858	5719	4.49	−0.23	57	−0.19	0.00
76151	5776	4.4	0.05	76151	5781	4.44	0.12	−5	−0.04	−0.07
125184	5695	4.3	0.31	125184	5660	4.11	0.27	35	0.19	0.04
146233	5799	4.4	0.01	146233	5810	4.46	0.05	−11	−0.06	−0.04
161098	5617	4.3	−0.27	161098	5574	4.49	−0.26	43	−0.19	−0.01
199960	5878	4.2	0.23	199960	5928	4.42	0.27	−50	−0.22	−0.04
210752	6014	4.6	−0.53	210752	5970	4.52	−0.55	44	0.08	0.02
	our				Mashonkina & Gehren (2001)					
4614	5965	4.4	−0.24	4614	5940	4.33	−0.3	25	0.07	0.06
22879	5972	4.5	−0.77	22879	5870	4.27	−0.86	102	0.23	0.09
55575	5949	4.3	−0.31	55575	5890	4.25	−0.36	59	0.05	0.05
64606	5250	4.2	−0.91	64606	5320	4.54	−0.89	−70	−0.34	-0.02
65583	5373	4.6	−0.67	65583	5320	4.55	−0.73	53	0.05	0.06
68017	5651	4.2	−0.42	68017	5630	4.45	−0.40	21	−0.25	−0.02
109358	5897	4.2	−0.18	109358	5860	4.36	−0.21	37	−0.16	0.03
112758	5203	4.2	−0.56	112758	5240	4.62	−0.43	−37	−0.42	−0.13
114710	5954	4.3	0.07	114710	6000	4.30	−0.03	−46	0.0	0.1
117176	5611	4.0	−0.03	117176	5480	3.83	−0.11	131	0.17	0.08
126053	5728	4.2	−0.32	126053	5690	4.45	−0.35	38	−0.25	0.03
144579	5294	4.1	−0.70	144579	5330	4.59	−0.69	−36	−0.49	−0.01
168009	5826	4.1	−0.01	168009	5785	4.23	−0.03	41	−0.13	0.02
176377	5901	4.4	−0.17	176377	5860	4.43	−0.27	41	−0.03	0.1
	our				Reddy et al. (2003)					
11007	5980	4	−0.2	11007	5850	4	−0.31	130	0	0.11
42618	5787	4.5	−0.07	42618	5653	4.58	−0.16	134	−0.08	0.09
45067	6058	4	−0.02	45067	5946	3.99	−0.12	112	0.01	0.1
71148	5850	4.2	0	71148	5703	4.46	−0.08	147	−0.26	0.08
126053	5728	4.2	−0.32	126053	5597	4.44	−0.41	131	−0.24	0.09
186408	5803	4.2	0.09	186408	5670	4.32	0	133	−0.12	0.09
206860	5927	4.6	−0.07	206860	5820	4.48	−0.12	107	0.12	0.05
	our				Brewer & Carney (2006)					
25665	4967	4.7	0.01	25665	4870	4.4	−0.012	97	0.3	0.022
53927	4860	4.64	−0.22	53927	4960	4.6	−0.385	−100	0.04	0.165
159062	5414	4.3	−0.4	159062	5260	4.45	−0.507	154	−0.15	0.107
168009	5826	4.1	−0.01	168009	5720	4.2	−0.07	106	−0.1	0.06

Table 2. Comparison of our parameters and Sr abundance determinations with the results of other authors for the *n* stars shared with our stellar sample.

Reference	$\Delta(T_{\rm eff})$	$\Delta(\log g)$	Δ([Fe/H])	Δ([Sr/Fe])	*n*
Battistini & Bensby	4	0.13	0.03	− 0.01	17 (1)
2016	±116	±0.15	±0.07	–	
Delgado Mena et al.	27	− 0.08	− 0.01	− 0.05	12
2017	±36	±0.13	±0.03	±0.09	
Mashonkina & Gehren	26	− 0.10	0.03	0.02	14
2001	±56	±0.21	±0.06	±0.10	
Reddy et al.	127	− 0.08	0.09	− 0.03	7
2003	±13	±0.14	±0.02	±0.08	
Brewer & Carney	64	0.02	0.09	− 0.21	4
2006	±112	±0.20	±0.06	±0.22	

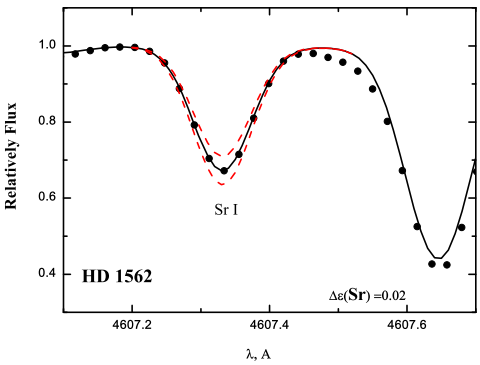

Figure 1. Observed (dots) and calculated (solid and dashed lines) spectra in the region of the Sr I line for HD 1562; the change in the Sr abundance is 0.02 dex.

3 DETERMINATION OF SR ABUNDANCES

The determination of the Sr abundance was obtained with the new version of the STARSP LTE spectral synthesis code (Tsymbal 1996) from the Sr I line at 4607 Å using the stellar models (Castelli & Kurucz 2004). A comparison of synthetic and observed spectra for the Sr line is shown in Fig. 1.

The Sr abundance was determined by differential analysis relative to the solar one. Solar abundances were calculated using the solar profiles measured in the spectra of the Moon and asteroids; they were also estimated using the SOPHIE spectrograph and the oscillator strengths log *gf* adopted from the Vienna Atomic Line Database (VALD) database (Kupka F. et al. 1999). Our approved LTE solar Sr abundance is $\log A(\mathrm{Sr})_{\odot} = 2.74 \pm 0.03$, in comparison with 2.87 ± 0.07 (Asplund et al. 2009), 2.83 ± 0.06 (Grevesse et al. 2015) and 2.78 (Delgado Mena et al. 2017). It should be emphasized that in Battistini & Bensby (2016) the values of the solar Sr abundance determined from the 4607-Å line in the spectra of reflected sunlight obtained from different spectrographs with various resolutions are given. These values noticeably different (about 0.2 dex), ranging from $\log A(\mathrm{Sr})_{\odot}$(MIKE) = 2.69 to $\log A(\mathrm{Sr})_{\odot}$(FEROS) = 2.92, where $\log A(\mathrm{H}) = 12.0$. This is important to keep in mind and take into account when determining the content of elements relative to the solar one, since it may generate a systematic shift of observational data. The departures from LTE and their effect on the determination of the Sr abundances for stars with different metallicities have been investigated in a number of articles (e.g. Belyakova & Mashonkina 1997; Mashonkina & Gehren 2001; Andrievsky et al. 2011), wherein the Sr II lines were analysed. An NLTE analysis of Sr I and Sr II lines in the spectra of late-type stars was performed by Bergemann et al. (2012). The model of the Sr atom was constructed using the atomic data available in the Hannover and NIST databases. The neutral atom was represented by 141 levels; the singly ionized atom included 49 levels. The described model of Sr was similar to that created by Andrievsky et al. (2011) with regard to the term structure and the number of dipole-permitted transitions of Sr II, but unlike the latter it factored in the effect of deviations from LTE on the neutral Sr line (for more details see Bergemann et al. 2012). A grid of the NLTE abundance corrections for Sr I and Sr II lines was presented in Bergemann et al. (2012). The NLTE corrections for the Sr I line at 4607 Å reported in Bergemann et al. (2012) for dwarfs varied within the range 0.10–0.23 dex at [Fe/H] > –0.8 dex, depending on the temperature and metallicity of the star. Using the data of Bergemann et al. (2012), we have interpolated the values of the NLTE corrections for the Sr I line at 4607 Å for our target stars. The NLTE Sr correction for the Sun is 0.10 dex. For metal-poor stars, it is more suitable to use the Sr II lines, which have smaller NLTE corrections, not exceeding 0.2 dex (Andrievsky et al. 2011) or close to 0.05 dex (Hansen et al. 2013).

The obtained LTE Sr abundances, the NLTE corrections from Bergemann et al. (2012), the NLTE Ba and LTE Eu abundances and stellar parameters (Mishenina et al. 2013) are given in Table A1.

Fig. 4 presents our observations and a comparison with GCE predictions by Bisterzo et al. (2014) and Travaglio et al. (2004), and also the interpolated NLTE corrections from Bergemann et al. (2012). Fig. 5 shows a comparison between our data and those of Battistini & Bensby (2016) and Delgado Mena et al. (2017) with the GCE model by Bisterzo et al. (2014).

3.1 Errors in abundance determinations

To determine the systematic errors in the elemental abundances resulting from uncertainties in the atmospheric parameters, we derived the elemental abundances of two stars HD 216259 ($T_{\rm eff}$ = 4833 K, log *g* = 4.60, $V_{\rm t}$ = 0.5 km s^{-1}, [Fe/H] = −0.55) and HD 9826 ($T_{\rm eff}$ = 6074 K, log *g* = 4.00, $V_{\rm t}$ = 1.3 km s^{-1}, [Fe/H] = 0.10) for several models with modified parameters ($\Delta T_{\rm eff}$ = ±100 K, Δlog *g* = ±0.2, $\Delta V_{\rm t}$ = ±0.1). The abundance variations with the modified parameters and the fitting errors for the computed and observed spectral line profiles (0.02 dex) are given in Table 3. The maximum contribution to the error is introduced by $T_{\rm eff}$. Total errors due to parameter uncertainties and the measured spectra vary from 0.12 dex for hot to 0.06–0.17 dex for cool stars. The dependence of the Sr abundance on stellar parameters ($T_{\rm eff}$ and log *g*) is presented in Figs 2 and 3. No trend of [Sr/Fe] versus $T_{\rm eff}$ and log *g* is

Table 3. Abundance errors due to atmospheric parameter uncertainties as examples of stars with different values of stellar parameters: HD 216259 (4833, 4.60, 0.5, −0.55) and HD 9826 (6074, 4.00, 1.3, 0.10).

		HD 216259				HD 9826			
AN	El	$\Delta T_{\rm eff}$ +	$\Delta \log g$ +	$\Delta V_{\rm t}$ +	tot +	$\Delta T_{\rm eff}$ +	$\Delta \log g$ +	$\Delta V_{\rm t}$ +	tot +
38	SrI	0.15	−0.07	−0.04	0.17	0.12	0.00	−0.02	0.12

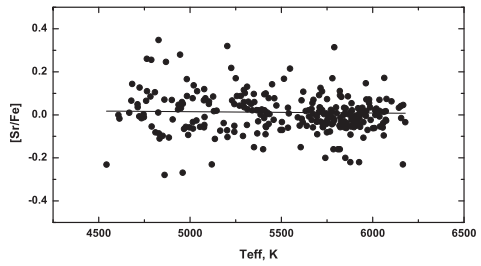

Figure 2. Dependence of [Sr/Fe] versus $T_{\rm eff}$.

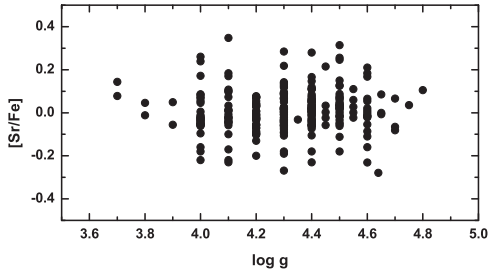

Figure 3. Dependence of [Sr/Fe] versus log g.

observed.

We compare our LTE Sr abundances with the ones obtained by Battistini & Bensby (2016) in the LTE assumption, using the same Sr I line, 4607 Å, as in our case. We have only one star in common (HD 64606) with that work, for which the Sr abundance is provided. The difference in the Sr abundance of HD 64606 is consistent within 0.01 dex. The mean value of the difference between our LTE definitions and those of Delgado Mena et al. (2017) is equal to –0.05 ± 0.09, confirming the overall agreement with our determinations. For five stars (HD 22049, HD 22879, HD 38858, HD 125184, HD 161098), the individual differences are larger than 0.05 dex, as highlighted in Fig. 5. As can be seen from the figures, a significant scatter in [Sr/Fe] ratio is observed. In our stellar sample, we obtain an observed range $-0.28 \lesssim$ [Sr/Fe] $\lesssim 0.34$ for thin-disc stars, which is higher than the range measured for more metal-poor thin-disc stars ($-0.03 \lesssim$ [Sr/Fe] $\lesssim 0.26$ dex). This is likely due to a smaller sample of metal-poor stars, providing a less meaningful comparison. We have good agreement with the results by Delgado Mena et al. (2017) for thin-disc stars with solar-like metallicity ($-0.19 \lesssim$ [Sr/Fe] $\lesssim 0.29$ dex), while they obtain a larger scatter for Sr abundances in metal-poor stars ($-0.36 \lesssim$ [Sr/Fe] $\lesssim 0.40$ dex). Greater variation of Sr abundances is shown by Battistini & Bensby (2016) ($-0.37 \lesssim$ [Sr/Fe] $\lesssim 0.54$ dex). Their results are obtained in the LTE approximation, but the NLTE corrections are positive, meaning that NLTE corrections will not improve the situation for moderately metal-poor stars. Taking into account observational data for [Sr/Fe] and their uncertainties, the observed dispersion of [Sr/Fe] is larger than the errors provided: ± 0.15 dex for our determinations, consistent with Battistini & Bensby (2016), and from 0.01–0.46 dex for the stellar data by Delgado Mena et al. (2017). Concerning the [Sr/Fe] trend with respect to [Fe/H], based on our data for thin and thick discs we did not find any significant trend (slope -0.00379 ± 0.02427). Battistini & Bensby (2016) instead reported a mild increasing [Sr/Fe] abundance ratio with decreasing metallicity: [Sr/Fe] ≈ -0.2 for solar metallicity stars, increasing to [Sr/Fe] ≈ 0 at [Fe/H] ≈ 1. Taking into account the large [Sr/Fe] scatter observed in metal-poor stars, giants and dwarfs (e.g. Burris et al. 2000; Brewer & Carney 2006), over a metallicity range $-2.0 <$ [Fe/H] < 0.2, the trend seems to be solar on average (e.g. Brewer & Carney 2006). Ishigaki, Aoki & Chiba (2013) observed thick-disc and halo stars, also finding solar [Sr/Fe] ratios for [Fe/H] < -1. While there may be contradictory results concerning the observational trend of [Sr/Fe], especially for metal-poor stars in the thick disc and halo, a significant real [Sr/Fe] dispersion beyond the observational error is a consistent result obtained from all authors.

As shown in various works (e.g. Belyakova & Mashonkina 1997; Mashonkina & Gehren 2001; Andrievsky et al. 2011; Bergemann et al. 2012), the NLTE corrections for the lines of neutral and ionized strontium depend on the stellar parameters ($T_{\rm eff}$, log g and [Fe/H]). Specifically, the dependence on metallicity affects estimates of the strontium abundance in various Galactic substructures, primarily the halo and the disc, which differ in this parameter. For stars of the lowest metallicity (halo), the Sr II line is usually used to determine the strontium abundance, for which NLTE corrections are small (e.g. Andrievsky et al. 2011). The use of the Sr I lines requires NLTE corrections from 0.05–0.5 (e.g. Bergemann et al. 2012), depending on the metallicity. As we show in Fig. 4, in our considered metallicity range, the average value of NLTE corrections is 0.151 dex for stars of the thin disc; for stars of the thick disc this changes from 0.137 to 0.244 dex and there is a dependence on metallicity. Consideration of the Sr abundance behaviour in thin- and thick-disc stars has shown that NLTE deviations change the trend more for thick-disc stars than for thin-disc stars. However, the scatter of the Sr abundance for all metallicities of the disc (and the Galaxy) does not allow a fine comparison of the Sr abundance in various substructures of the disc with predictions of models of Galactic evolution.

4 RESULTS AND COMPARISON WITH GCE MODELS

Element abundances measured in stars are an ideal yardstick for nucleosynthesis predictions and their effect on stellar and galactic evolution. The Solar system abundance of the element Sr is dominated by the *s*-process contribution to ^{88}Sr (82.6 per cent of the solar Sr) by AGB stars. ^{86}Sr and ^{87}Sr (9.9 per cent and 7.0 per cent of the solar Sr, respectively) are *s*-only isotopes (Käppeler et al. 2011). Finally, the rarest Sr isotope is ^{84}Sr (0.56 per cent of the solar Sr), which is a product of the *p*-process in stars (e.g. Rauscher et al. 2013; Pignatari et al. 2016a; Travaglio et al. 2018, and references therein).

As discussed in the Introduction, a zoo of different nucleosynthesis processes can contribute to the production of Sr stable iso-

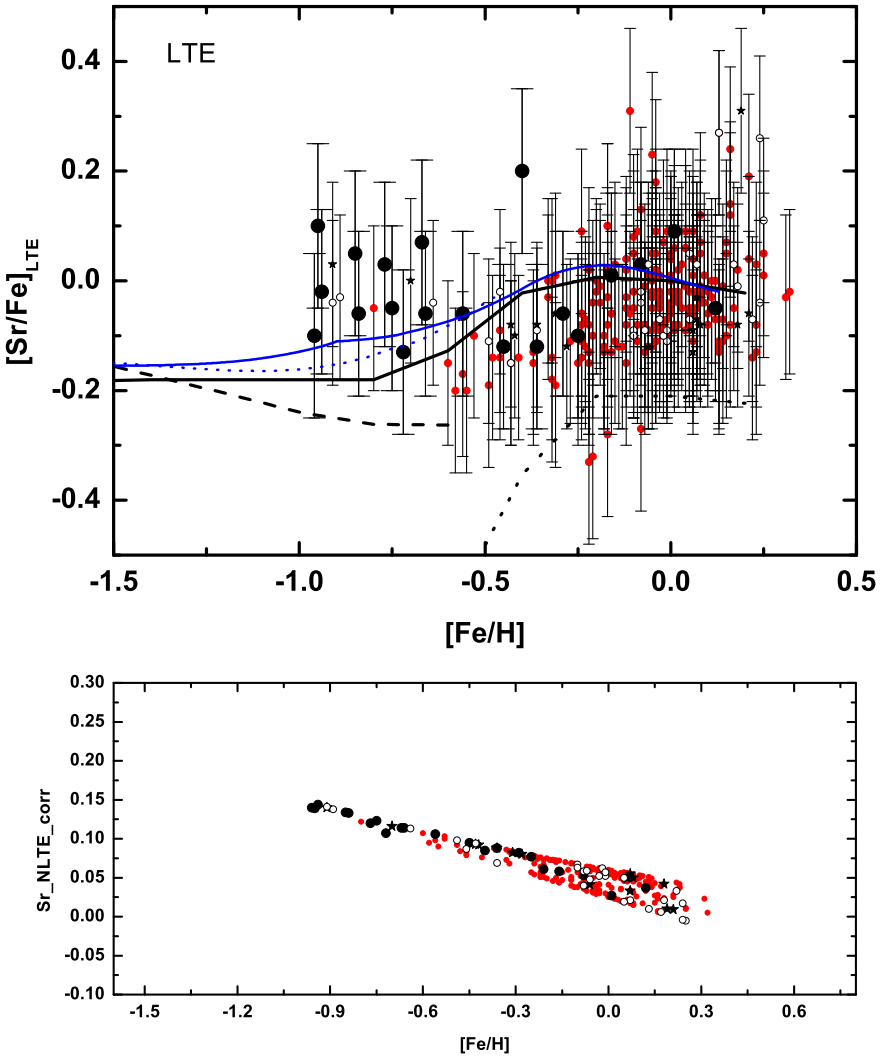

Figure 4. Our determined LTE (upper panel) Sr abundances (thin disc: small circles, thick disc: circles, Hercules stream: asterisks, unclassified: open circles) and a comparison with models of Bisterzo et al. (2014) (thin disc: line, thick disc: dotted line) and Travaglio et al. (2004) (thin disc: thick line, thick disc: thick dashed line, only s-process contribution: thick dotted line). NLTE corrections are from Bergemann et al. (2012) (bottom panel).

topes. Since spectroscopic observations can only determine element abundances for Sr, no constraints on the isotopic pattern exist, except for the Sun. Therefore, it becomes difficult to disentangle the contribution from these different processes in stars in Galactic archaeology studies (e.g. Yong et al. 2013), where few or even only one single nucleosynthesis event could dominate the isotopic abundance pattern. Sr is often used as a tracer of LEPP enrichment in metal-poor stars (e.g. Montes et al. 2007). However, Sr elemental observations may lead to different interpretations. Fröhlich et al. (2006) suggested the *vp*-process as a source of nuclei up to $A = 90$ or slightly beyond, originating in the neutrino-driven winds from forming neutron stars in CCSNe (see also the more recent investigations by Martínez-Pinedo et al. 2014; Eichler et al. 2017). Due to the electron fraction Y_e being larger than 0.5, the *vp*-process acts on the proton-rich side of the valley of stability, producing a non-solar isotopic pattern. The weak *s*-process, activated by the ^{22}Ne neutron source in massive stars, is usually metallicity-dependent and negligible at low metallicities. However, in fast-rotating massive stars ^{14}N can be made by rotational mixing, leading to a primary production of ^{22}Ne in He-burning. The *s*-process production in fast-rotating massive stars has been investigated (Pignatari et al. 2008; Frischknecht et al. 2016; Choplin et al. 2017; Meynet & Maeder 2017; Nishimura et al. 2017; Prantzos et al. 2018) and considered by GCE modelling (Cescutti et al. 2015a; Bisterzo et al. 2017; Prantzos et al. 2018). On the other hand, as mentioned in the Introduction, the existence of the LEPP component is controversial (Cristallo et al. 2015; Trippella et al. 2016; Prantzos et al. 2018). A consistent set of observations over a large sample of stars such as the one presented in this work becomes instrumental to shed more light in this debate.

Our results for the Sr abundance obtained within the LTE approximation and the NLTE corrections (Bergemann et al. 2012) for our Sr determinations are shown in Fig. 4, in comparison with GCE model results from Travaglio et al. (2004) and Bisterzo et al. (2017). This GCE model (Travaglio et al. 2004) follows the composition of stars, stellar remnants, interstellar matter (atomic and molecular gas) and their mutual interaction in the three main zones of the Galaxy: halo, thick disc and thin disc. The chemical enrichment takes into account the *s*-process yields from AGB stars, the *r* contribution from massive stars (estimated with the residual method $Nr = N_{\odot} - Ns$) and the primary LEPP contribution. As

discussed in Travaglio et al. (2004), the impact of AGB uncertainties on GCE computations may be partially reduced by assuming a range of ^{13}C-pocket strengths, according to the *s*-process spread observed in disc stars and presolar meteoritic SiC grains. The *r* contribution was assumed to derive from SNe II of mass 8–10 $M_{\odot}$. Nevertheless, we do not exclude different hypotheses to explore the chemical origin of the Galactic halo (e.g. see discussion in Section 1). The LEPP contribution was evoked to explain the missing abundance of solar Sr; the ffiat [Sr/Fe] trend observed at low metallicities suggested that LEPP is a primary process, likely occurring in CCSNe with an extended range of mass progenitors compared with the main *r*-process. In Fig. 4, the Galactic disc predictions by Travaglio et al. (2004) are represented by a thick line for the thin disc and a dashed thick line for the thick disc. Note that models that consider only the contribution to neutron-capture enrichment from *s*- and *r*- processes do not reproduce the observations at low metallicity (dotted line).

In Figs 4 and 5, GCE calculations by Bisterzo et al. (2017) are compared with the observations (thin disc: line, thick disc: dotted line). The Bisterzo et al. (2017) simulations included new stellar yields and GCE parameters compared with Travaglio et al. (2004). In particular, GCE Fe predictions by Bisterzo et al. (2017) are obtained by using SN Ia stellar yields from Travaglio, Hillebrandt & Reinecke (2005), coupled with an updated treatment of the delayed-time distribution function as suggested by Kobayashi et al. (1998), Kobayashi, Nomoto & Hachisu (2015), Greggio (2005) and Matteucci et al. (2009), in which we assume a dominant SN Ia contribution starting from [Fe/H] > -1.

Bisterzo et al. (2017) also investigate the impact on GCE simulations of the internal structure of the ^{13}C pocket, which is one of the major uncertainties for *s*-process production in AGB stars. Considering these uncertainties, the authors confirmed their earlier results (Travaglio et al. 2004), where an additional LEPP contribution is required in order to represent the solar *s*-process abundances of isotopes from $A = 90$–130 (solar LEPP, Montes et al. 2007). Bisterzo et al. (2017) also discussed the impact of the *s*-process yields from fast-rotating massive stars, with a contribution of up to $\sim$ 17 per cent to solar Sr (*s*-process yields from fast-rotating massive star yields by Frischknecht et al. 2016). Therefore, according to those calculations, the maximum *s*-process production of Sr is $Sr_s \sim 90$ per cent. Instead, *s*-process isotopes and elements with $90 < A < 130$ are marginally affected by this additional source of *s*-process, with variations within the solar uncertainties.

GCE simulations presented in the figure can reproduce Sr production in the Galaxy and solar abundances of Sr. In particular, by also considering the contribution from fast-rotating massive stars, the [Sr/Fe] abundance in thin-disc stars is better reproduced compared with Travaglio et al. (2004). On the other hand, the production of Y and heavier LEPP elements is not obtained; they are possibly made by a combination of other nucleosynthesis processes.

In Fig. 6 we show the evolution of the [Sr/Ba] and [Sr/Eu] ratios with respect to [Fe/H]. The average observational error is reported in the figures. The abundances for Ba and Eu were taken from Mishenina et al. (2013). Ba abundances were computed under the NLTE approximation in our earlier studies (Korotin et al. 2011; Mishenina et al. 2013). Ba abundances in dwarf stars were determined from Ba II 4554, 5853, 6141 and 6496 Å, while the LTE Eu abundance was derived from the line at 6645 Å (Mishenina et al. 2013). The NLTE profiles of the Ba lines were computed using a modified version of the MULTI code (Carlsson 1986); all modifications have been described in detail in Korotin, Andrievsky & Luck (1999). The Ba model in this study contains 31 levels of Ba I, 101 levels of Ba II with $n < 50$ and the ground level of Ba III. The analysis covers 91 bound–bound transitions. The NLTE Ba calculations have been described in detail in Korotin et al. (2011). In order to verify the effect of LTE deviations on the Sr abundance, as well as on their relationship with other elemental abundances, we have plotted [Sr/Eu] versus [Fe/H] using both the NLTE and LTE Sr abundances. As can be seen in Fig. 6, there is no significant difference. A pure *r*-process signature has been indicated for both [Sr/Ba] and [Sr/Eu], assuming that $Sr_r = 9$ per cent of the solar Sr abundance. This estimation is based on observations of very metal-poor *r*-process rich stars (Travaglio et al. 2004; Mashonkina & Christlieb 2014; Roederer et al. 2014). We therefore use $Ba_r = 15$ per cent of the solar Ba content and $Eu_r = 94$ per cent of the solar Eu abundance (using the residual method and the GCE *s*-process calculations by Bisterzo et al. 2017). The *r*-process contribution to Ba and Eu in the solar composition is derived by subtracting the *s*-process fractions from the solar abundances (*r*-process residuals method).

The $[Sr/Eu]_r$ ratio is well below that of any star observed in the Galactic disc, confirming that other early nucleosynthesis processes producing Sr are contributing. The $[Sr/Ba]_r$ ratio is close to the solar ratio and not much information can be derived. In Fig. 7, the [Sr/Ba] (NLTE) ratio is shown with respect to the [Ba/Eu] (NLTE Ba, LTE Eu) ratio. Ratios consistent with the *r*-process production and the *s*-process contribution are shown for comparison. Most of the stars show abundance signatures consistent with a combined contribution of the *s*-process and *r*-process. Also in the Galactic disc, for a number of stars we can see a possible signature similar to the stellar LEPP (Montes et al. 2007), where [Sr/Ba] is larger than the *s*-process contributions and the *r*-process and consistent with the results of François et al. (2007), where anti-correlations of [Sr/Ba], [Y/Ba] and [Zr/Ba] ratios with $4.5 <$ [Ba/H] < 1.5 were obtained. These results confirm the need for additional nucleosynthesis processes responsible for synthesis of the first-peak elements. Andrievsky et al. (2011) have reanalysed Sr and Ba abundances from François et al. (2007) in the NLTE approximation and have compared this with the theoretical predictions of the LEPP model (Travaglio et al. 2004). Their NLTE homogeneous determinations qualitatively confirm the Sr, Y, Zr and Ba behaviour found in François et al. (2007) and enable one to claim robustly that the Sr abundances are generally higher than those predicted by the main *r*-process pattern. They have concluded that, since the theoretical curve of a LEPP process is not far from the upper envelope of their data points, an inhomogeneous mixing of the products of such a LEPP process with the products of the main *r*-process could explain the distribution of studied metal-poor stars. In our figures, the stars with the highest [Sr/Ba] are less than 0.3 dex beyond the *s*-process prediction. This might be seen as a signature of the different nucleosynthesis processes contributing to Sr and discussed before for Galactic archaeology studies, but this scatter is close to the [Sr/Ba] observational error. Four stars have a ratio of [Sr/Ba] (Sr and Ba abundances presented in NLTE approach) higher than 0.3 dex: namely HD 64606 ([Sr/Fe] = 0.17, [Sr/Ba] = 0.31), HD 139323 ([Sr/Fe] = 0.32, [Sr/Ba] = 0.32), HD 144579 ([Sr/Fe] =0.11, [Sr/Ba] = 0.37) (Hercules stream) and HD 32147 ([Sr/Fe] = 0.28, [Sr/Ba] = 0.32) belong to the category of unclassified stars. These stars have a different kinematics from the stars of thick and thin discs and this could provide a reason to consider their special enrichment with Sr. However, only two of them show some excess of Sr, slightly exceeding the determination errors. Interestingly, there are five stars with [Sr/Ba] ratio falling outside the range of errors from the *s*-process or *r*-process: HD 26923 ([Sr/Ba] = −0.249 LTE, 0.03 NLTE), HD 45088 (−0.309, −0.269), HD 53927 (−0.259, −0.279),

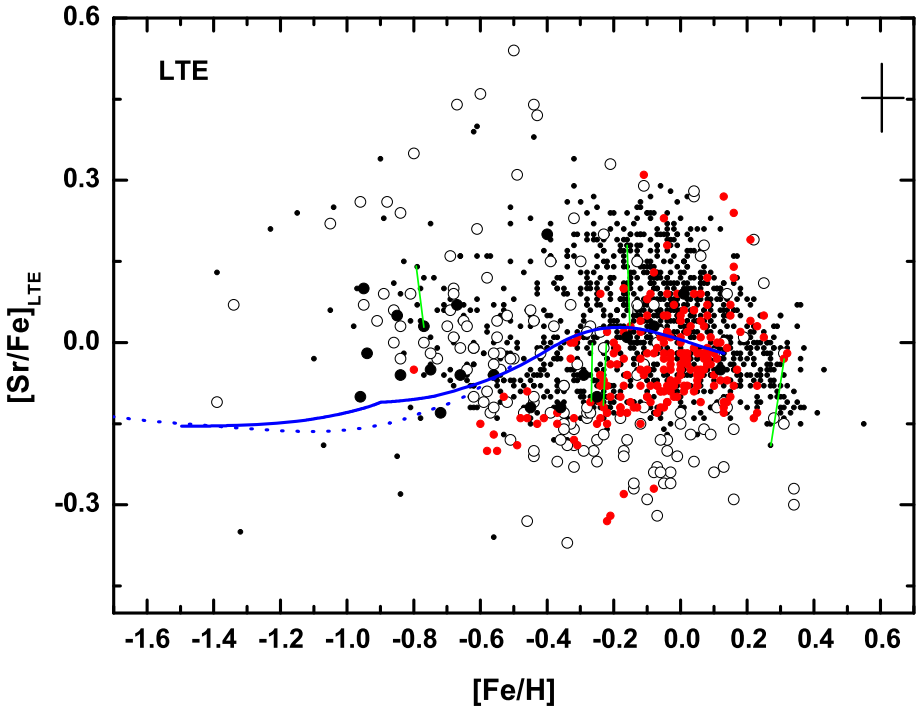

Figure 5. A comparison of our [Sr/Fe] LTE (thin disc: small circles, thick disc: circles) with the data of Battistini & Bensby (2016) (open circles), Delgado Mena et al. (2017) (points) and the chemical evolution prediction by Bisterzo et al. (2017) (thin disc: line, thick disc: dotted line).The values of the Sr abundance obtained by us and in other works that are different by more than 0.1 dex are connected (marked) by lines.

HD 127506 (−0.191, −0.231), HD 141272 (−0.187, −0.047). The [Sr/Ba] ratios for each star are given in parentheses, wherein the first value corresponds to the LTE Sr abundance and the second value corresponds to the NLTE Sr content; for Ba, the NLTE abundance estimates are used in both cases. For three stars, HD 45088, 53927 and 127506, these deviations are the same for both the LTE and NLTE Sr abundance determinations. Again, we are quite close to the error range limit. The same uncommon signature is observed in a few metal-poor stars (e.g. Roederer et al. 2010; Frebel 2010; Hansen et al. 2018), indicating the contribution from different *r*-process components or some additional nucleosynthesis component that is not taken into account in this analysis.

In Fig. 8, we have compared our [Sr/Fe] LTE data and those obtained in numerous studies within a large range of [Fe/H] with GCE predictions by Bisterzo et al. (2017) and Prantzos et al. (2018). The evolution computed from Bisterzo et al. (2017) is marked for the thin disc as a line and for the thick disc as a dotted line (Fig. 8). The predicted evolution (Prantzos et al. 2018) is shown for cases wherein different contributing sources were considered: (i) low- and intermediate-mass (LIM) stars, rotating massive stars plus their fiduciary *r*-process (the baseline model, dashed curve); (ii) LIM stars, non-rotating massive stars and *r*-process (short dashed curve); (iii) LIM stars and non-rotating massive stars without *r*-process contribution (short dotted curve); (iv) LIM stars plus rotating massive stars without *r*-process contribution (dash-dotted curve). The authors have drawn the conclusion that, overall, the computed [*X*/Fe] versus [Fe/H] evolution for the *s*-elements is consistent with the evolution predictions made in previous studies (e.g. Bisterzo et al. 2017) for metallicities typical of the disc ([Fe/H] ≥ -1.0), but the weak *s*-process in rotating massive stars plays a key role in the evolution of *s*-elements at low metallicity. Note that the extra source of neutron-capture elements required to explain solar abundances, which led Travaglio et al. (2004) to postulate an additional process (LEPP), could apparently be explained by Prantzos et al. (2018) as a contribution from rotating massive stars.

As can be seen in the figures, there is a large scatter of Sr abundances at all metallicities, including near-solar ones, which are of specific interest in this study. The resulting spread exceeds the observation errors, as well as the differences obtained in various studies applying different approaches (e.g. using LTE or NLTE assumptions). In order to evaluate the description of the observational data by various calculations (using different models) of GCE, we have presented our observations and those obtained by Battistini & Bensby (2016) and Delgado Mena et al. (2017) as a single data set and expressed them as a third-degree polynomial to plot versus the average observational trend. Fig. 9 illustrates the average observational trend with the error-function determination by a polynomial, as well as models developed by Bisterzo et al. (2017) and Prantzos et al. (2018). We have displayed the predicted evolution of Bisterzo et al. (2017) (for the thin disc as a line and the thick disc as a dotted line) and those of Prantzos et al. (2018) for cases wherein different contributing sources were considered: (a) low- and intermediate-mass (LIM) stars, rotating massive stars and *r*-process contribution (the baseline model, dashed curve) and (b) LIM stars plus rotating massive stars without the *r*-process contribution (dot-dashed curve). Indeed the computed [Sr/Fe] versus [Fe/H] evolution is fully consistent with the predictions made by Bisterzo et al. (2017) and Prantzos et al. (2018) for metallicities typical for disc stars ([Fe/H] ≥ -1.0). The main difference between the adopted models is due to the different contribution to the chemical enrichment from

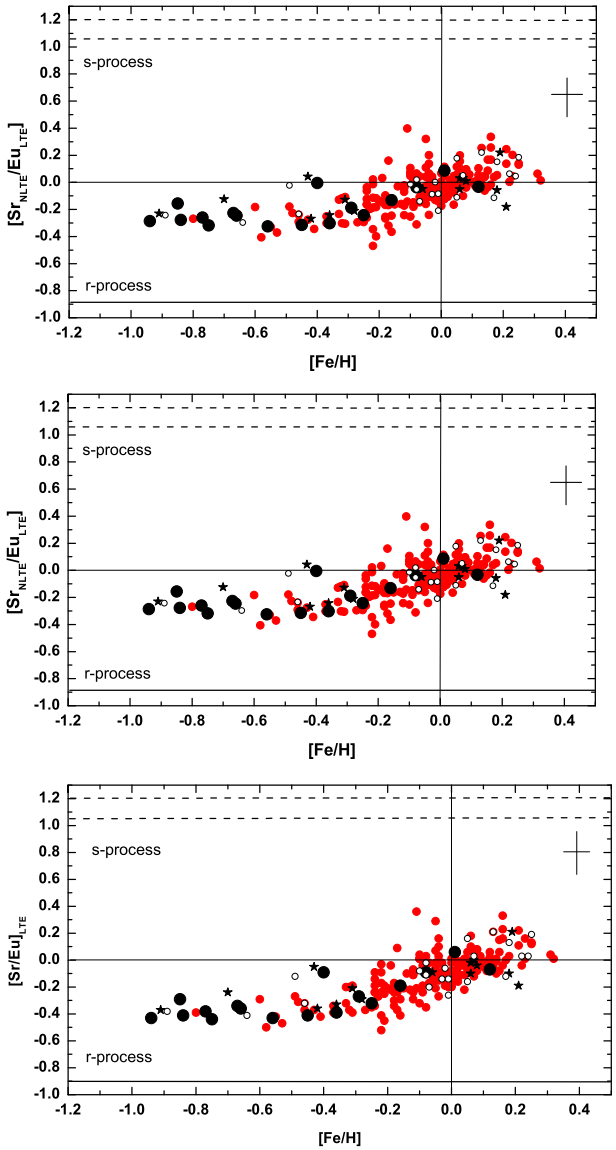

Figure 6. Dependences of [Sr/Ba] (NLTE), [Sr/Eu] (Sr NLTE data) and [Sr/Eu] (Sr LTE data) versus [Fe/H] with *r*-, *s*- process introduction from Bisterzo et al. (2017). The *s*-process signatures (pure AGB *s*-process production and including *s*-process contribution from massive stars) and *r*-process signatures are included: $[Sr/Ba]_r = -0.10$; $[Sr/Eu]_r = -0.89$; $[Ba/Eu]_r = -0.80$; $[Sr/Ba]_s = -0.09$ (pure AGB) to +0.05 (AGB + massive stars); $[Sr/Eu]_s = 1.06$ (pure AGB) to 1.20 (AGB + massive stars); $[Ba/Eu]_s = 1.15$. Notations are as follows: thin-disc stars marked as small circles, thick-disc stars as circles, Hercules stream stars as asterisks, non-classified stars as small open circles; *r*-process as a solid line, *s*-process as dotted lines.

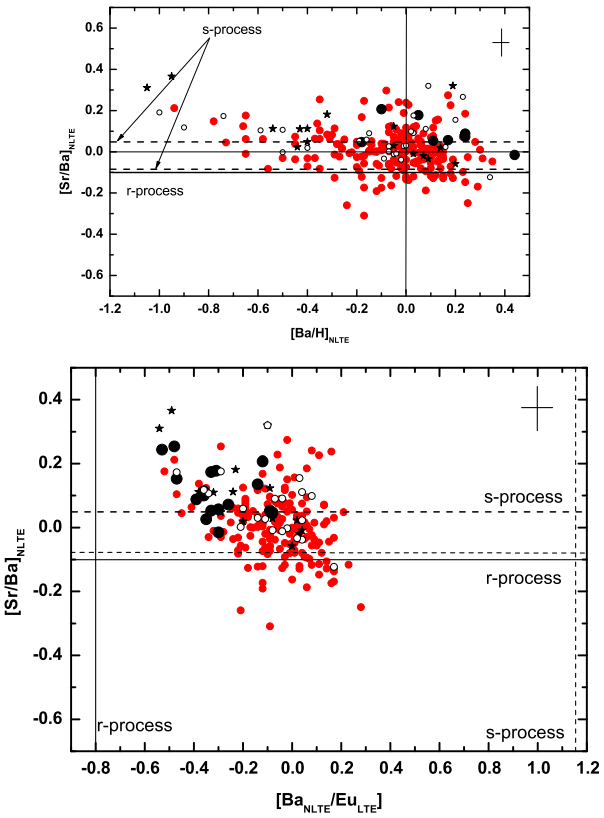

Figure 7. The [Sr/Ba] ratio (NLTE Sr, Ba) is shown with respect to [Ba/H] (NLTE Ba) and [Ba/Eu] (NLTE Ba, LTE Eu with *r*-, *s*- process introduction from Bisterzo et al. (2017). Notations are the same as in Fig. 6.

massive rotating stars. However, differences in the Sr abundance evolution in these two models are still within the accuracy of observations.

5 CONCLUSIONS

We present a new set of Sr abundances measured for 276 stars, including 212 thin-disc stars, 21 thick-disc stars, 16 Hercules stream stars and 27 non-classified stars. By the time this study began, the Sr abundances had been determined for less than 2 per cent of the stars in our sample. The LTE approach was employed to estimate the abundances, whereby the departures from LTE were determined using the results of Bergemann et al. (2012); the average NLTE correction was 0.15 dex. Comparison of our data with those of other authors showed good agreement between them, with only five stars having a departure in [Sr/Fe] of more than 0.05 dex.

We obtain an observational scatter in the Sr abundance of the order of 0.2–0.3 dex, beyond the observational errors (0.12–0.17 dex, see Table 3), in agreement with previous works. For thin-disc stars, we obtain a scatter $-0.28 \lesssim [Sr/Fe] \lesssim 0.34$, which is higher than the same range measured for more metal-poor thick-disc stars ($-0.03 \lesssim [Sr/Fe] \lesssim 0.26$ dex). However, our sample of thick-disc stars is too limited to draw robust conclusions. No significant trend is observed for the [Sr/Fe] evolution with respect to [Fe/H]. We note that there is no significant difference between the LTE and NLTE trends, as can be seen in Fig. 6.

We compared our results with the GCE calculations by Travaglio et al. (2004), Bisterzo et al. (2017) and Prantzos et al. (2018). A number of stellar sources contributed to the production of Sr in stars. We considered the *s*-process contribution from AGB stars, massive stars and fast-rotating massive stars. Sr_s ranges from 69 per cent of the solar Sr due to AGB stars up to ∼90 per cent, where the massive star contribution is also taken into account. Based on observations of metal-poor *r*-process rich stars, the contribution to the solar Sr from the *r*-process is smaller than 10 per cent. The LEPP contribution was evoked to explain the missing abundance of solar Sr; the [Sr/Fe] trend observed at low metallicities suggested that LEPP is a primary process, likely occurring in CCSNe with

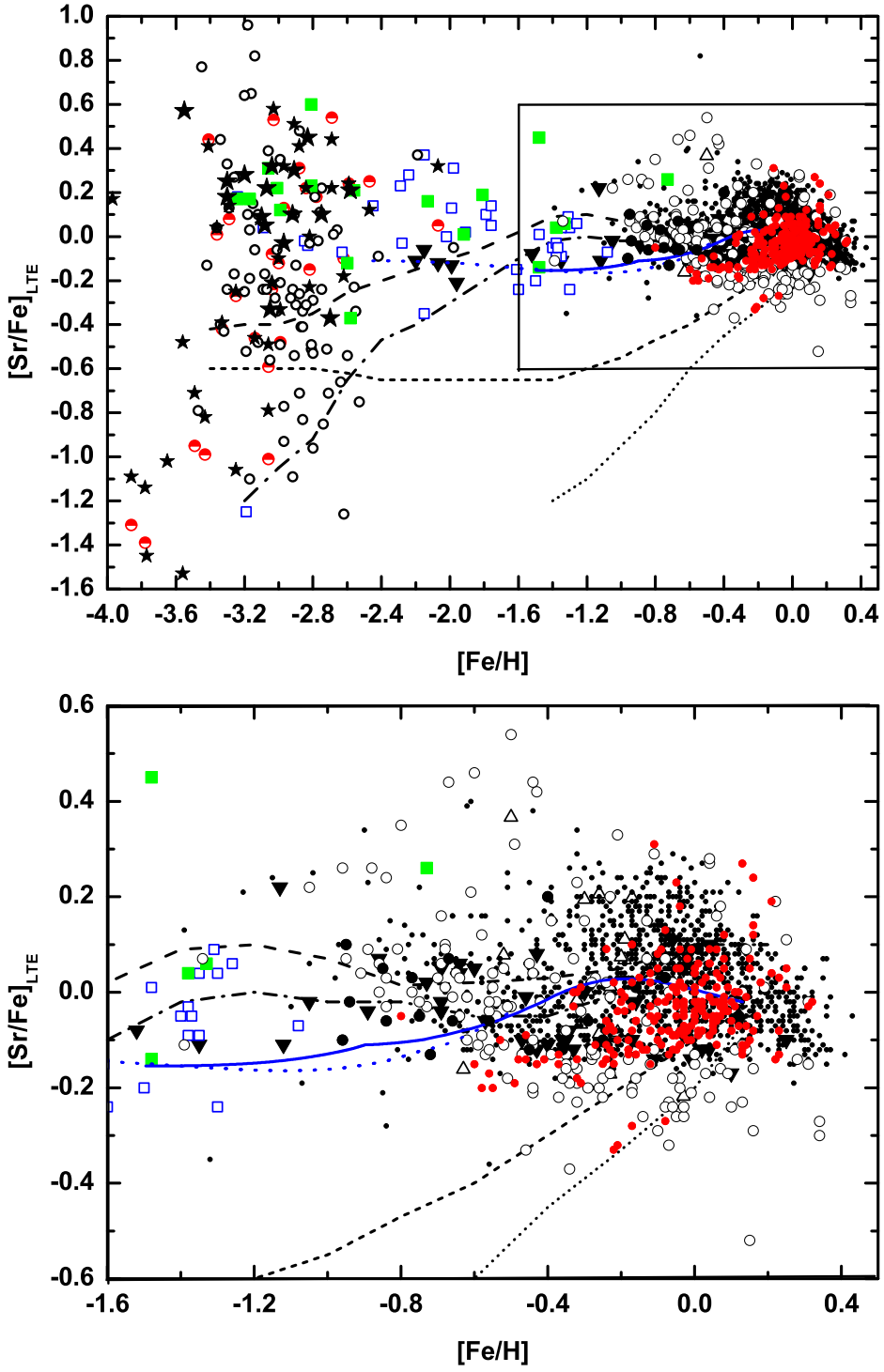

Figure 8. A comparison of our [Sr/Fe] LTE data and those of other works with GCE predictions with the chemical evolution predictions by Bisterzo et al. (2017) and Prantzos et al. (2018) (see model details in text). The data from different literature sources are marked as follows: our thin disc data as small circles, our thick disc data as circles; data from Mashonkina & Gehren (2001) as triangles; data from Brewer & Carney (2006) as open triangles, data from François et al. (2007) as semi-open circles, data from Andrievsky et al. (2011) as asterisks (small for turn-off stars, large for giants); data from Ishigaki et al. (2013) as open squares; data from Aoki et al. (2013) as small open circles; data from Hansen et al. (2013) as squares; data from Battistini & Bensby (2016) as large open circles; data from Delgado Mena et al. (2017) as small points.

an extended range of mass progenitors compared with the main *r*-process.

We have explored the Sr production together with Ba and Eu. We showed that, while most of the stars can be explained within the *s*-process and *r*-process residual paradigm, a fraction of stars with [Sr/Ba] higher than the upper limit of the Sr *s*-process contribution exists. While this feature is quite common in old stars formed in the early Galaxy, the observed departure from the *s*-process

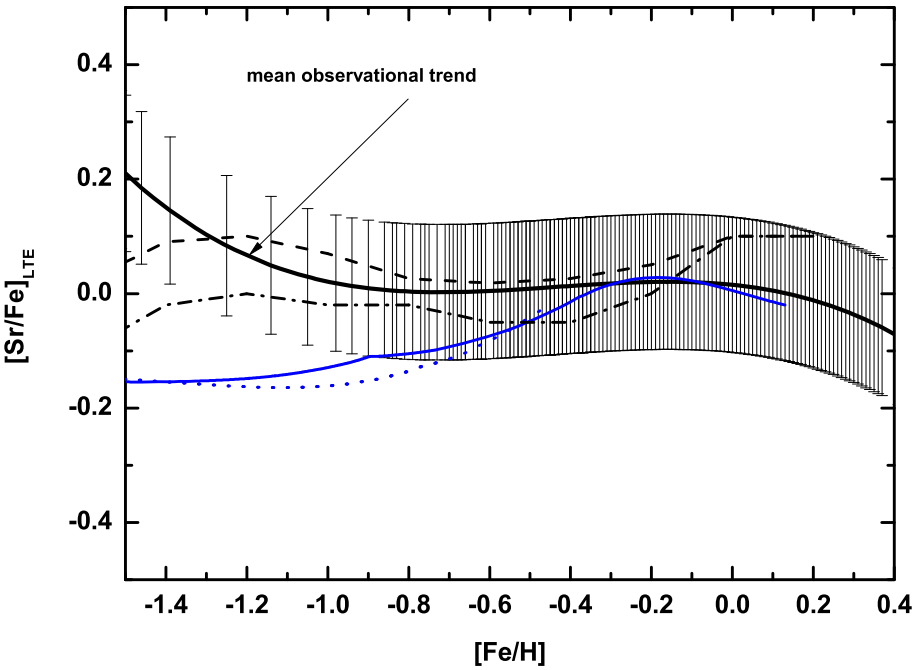

Figure 9. A comparison of the average observational [Sr/Fe] LTE data trend with the chemical evolution prediction by Bisterzo et al. (2017) and Prantzos et al. (2018) and in the Galactic disc range of [Fe/H].

limit of [Sr/Fe] is much weaker in Galactic disc stars, within the observational errors ($\sim$ 0.2 dex). We also obtain a small fraction of stars with [Sr/Ba] lower by up to 0.2 dex than the *r*-process. For at least three stars, both LTE and NLTE Sr abundances display values near -0.3 dex. Of course, taking the determination errors into account, this value is not so large, somewhere around 0.1 dex, which may be due to the dispersion of strontium and barium in the disc.

Using stellar data from our sample and from Battistini & Bensby (2016) and Delgado Mena et al. (2017), we have studied the production of Sr. Observations have been compared with GCE simulations by Bisterzo et al. (2017) and Prantzos et al. (2018). We confirm that the *s*-process contribution from AGB stars, massive stars and fast-rotating massive stars is the main source of Sr enrichment in the Galactic disc, possibly augmented by a CCSN contribution. The contribution of fast-rotating massive stars becomes more significant with decreasing metallicity.

A significant scatter in the [Sr/Fe] ratio is also seen in metal-poor stars, possibly indicating the contribution from additional *r*-process components in the early Galaxy (e.g. a main *r*-process contribution from rare events at low metallicities) and in the Galactic disc.

ACKNOWLEDGEMENTS

This article was based on observations collected at OHP Observatory, France. We thank Elisa Delgado Mena for providing the data before publishing. TM, TG, MP, FKT and SK are grateful for support from the Swiss National Science Foundation, project SCOPES No. IZ73Z0152485. MP acknowledges significant support of NuGrid from NSF grants PHY 09-22648 (Joint Institute for Nuclear Astrophysics, JINA) and PHY-1430152 (JINA Center for the Evolution of the Elements) and EU MIRG-CT-2006-046520. MP acknowledges support from the 'Lendület-2014' Programme of the Hungarian Academy of Sciences (Hungary), SNF (Switzerland), STFC (UK, through the University of Hull Consolidated Grant ST/R000840/1) and the VIPER HPC facility at the University of Hull (UK). FKT acknowledges support from the European Research Council (FP7) under ERC Advanced Grant Agreement 321263 FISH. SB thanks JINA (ND Fund 202476) for financial support. TM thanks O. Chepizhko for discussions. The authors are thankful to the anonymous referee for very useful comments.

REFERENCES

Allende Prieto C., García López R. J., Lambert D. L., Gustafsson B., 1999, ApJ, 527, 879
Andrievsky S. M., Spite F., Korotin S. A., François P., Spite M., Bonifacio P., Cayrel R., Hill V., 2011, A&A, 530, A105
Aoki W. et al., 2013, AJ, 145, 13
Aoki W., Beers T. C., Christlieb N., Norris J. E., Ryan S. G., Tsangarides S., 2007, ApJ, 655, 492
Arcones A., Montes F., 2011, ApJ, 731, 5
Asplund M., Grevesse N., Sauval A. J., Scott P., 2009, ARA&A, 47, 481
Battistini C., Bensby T., 2016, A&A, 586, A49
Belyakova E. V., Mashonkina L. I., 1997, Astron. Rep., 41, 530
Bergemann M., Hansen C. J., Bautista M., Ruchti G., 2012, A&A, 546, A90
Bisterzo S., Travaglio C., Gallino R., Wiescher M., Käppeler F., 2014, ApJ, 787, 10
Bisterzo S., Travaglio C., Wiescher M., Käppeler F., Gallino R., 2017, ApJ, 835, 97
Brewer M.-M., Carney B. W., 2006, AJ, 131, 431
Burris D. L., Pilachowski C. A., Armandroff T. E., Sneden C., Cowan J. J., Roe H., 2000, ApJ, 544, 302
Carlsson M., 1986, Uppsala Astronomical Observatory Reports, p. 33, Available at:http://adsabs.harvard.edu/abs/1986UppOR..33.....C
Castelli F., Kurucz R. L., 2004, preprint (astro-ph/0405087)
Cescutti G., Chiappini C., Hirschi R., Meynet G., 2015a, IAU General Assembly, 22, 2257239

Cescutti G., Romano D., Matteucci F., Chiappini C., Hirschi R., 2015b, A&A, 577, A139
Choplin A., Ekström S., Meynet G., Maeder A., Georgy C., Hirschi R., 2017, A&A, 605, A63
Clarkson O., Herwig F., Pignatari M., 2018, MNRAS, 474, L37
Cowan J. J., Rose W. K., 1977, ApJ, 217, 51
Cowan J. J., Sneden C., Lawler J. E., Aprahamian A., Wiescher M., Langanke K., Martínez-Pinedo G., Thielemann F.-K., 2019, preprint (arXiv:1901.01410)
Cristallo S., Abia C., Straniero O., Piersanti L., 2015, ApJ, 801, 53
Curtis S., Ebinger K., Fröhlich C., Hempel M., Perego A., Liebendörfer M., Thielemann F.-K., 2019, ApJ, 870, 2
D'Orazi V., De Silva G. M., Melo C. F. H., 2017, A&A, 598, A86
Dardelet L. et al., 2014, in Elekes Z., Fulop Z., eds, Proceedings of XIII Nuclei in the Cosmos (NIC XIII), Debrecen, Hungary, p. 145
Delgado Mena E., Tsantaki M., Adibekyan V. Z., Sousa S. G., Santos N. C., González Hernández J. I., Israelian G., 2017, A&A, 606, A94
Eichler M. et al., 2017, in Kubono S., Kajino T., Nishimura S., Isobe T., Nagataki S., Shima T., Takeda Y., eds, 14th International Symposium on Nuclei in the Cosmos (NIC2016), Niigata, Japan. p. 020604
Farouqi K., Kratz K.-L., Mashonkina L. I., Pfeiffer B., Cowan J. J., Thielemann F.-K., Truran J. W., 2009, ApJ, 694, L49
François P. et al., 2007, A&A, 476, 935
Frebel A., 2010, Astron. Nachr., 331, 474
Freiburghaus C., Rosswog S., Thielemann F.-K., 1999, ApJ, 525, L121
Frischknecht U. et al., 2016, MNRAS, 456, 1803
Fröhlich C., Hix W. R., Martínez-Pinedo G., Liebendörfer M., Thielemann F.-K., Bravo E., Langanke K., Zinner N. T., 2006, New Astron. Rev., 50, 496
Fujiya W., Hoppe P., Zinner E., Pignatari M., Herwig F., 2013, ApJ, 776, L29
Gaia Collaboration et al., 2018, A&A, 616, A11
Galazutdinov G. A., 1992, The processing system of stellar eshele spectra, Russian Academy of Sciences, Russia, p. 92
Gibson B. K., Fenner Y., Renda A., Kawata D., Lee H.-c., 2003, PASA, 20, 401
Goswami A., Prantzos N., 2000, A&A, 359, 191
Gratton R. G., Carretta E., Castelli F., 1996, A&A, 314, 191
Greggio L., 2005, A&A, 441, 1055
Grevesse N., Scott P., Asplund M., Sauval A. J., 2015, A&A, 573, A27
Hampel M., Stancliffe R. J., Lugaro M., Meyer B. S., 2016, ApJ, 831, 171
Hansen C. J., Bergemann M., Cescutti G., François P., Arcones A., Karakas A. I., Lind K., Chiappini C., 2013, A&A, 551, A57
Hansen C. J., Montes F., Arcones A., 2014, ApJ, 797, 123
Hansen T. T. et al., 2018, ApJ, 858, 92
Herwig F., Pignatari M., Woodward P. R., Porter D. H., Rockefeller G., Fryer C. L., Bennett M., Hirschi R., 2011, ApJ, 727, 89
Honda S., Aoki W., Kajino T., Ando H., Beers T. C., Izumiura H., Sadakane K., Takada-Hidai M., 2004, ApJ, 607, 474
Honda S., Aoki W., Ishimaru Y., Wanajo S., 2007, ApJ, 666, 1189
Ishigaki M. N., Aoki W., Chiba M., 2013, ApJ, 771, 67
Käppeler F., Gallino R., Bisterzo S., Aoki W., 2011, Rev. Modern Phys., 83, 157
Karakas A. I., Lattanzio J. C., 2014, PASA, 31, e030
Katz D., Soubiran C., Cayrel R., Adda M., Cautain R., 1998, A&A, 338, 151
Kobayashi C., Tsujimoto T., Nomoto K., Hachisu I., Kato M., 1998, ApJ, 503, L155
Kobayashi C., Karakas A. I., Umeda H., 2011, MNRAS, 414, 3231
Kobayashi C., Nomoto K., Hachisu I., 2015, ApJ, 804, L24
Korotin S., Mishenina T., Gorbaneva T., Soubiran C., 2011, MNRAS, 415, 2093
Korotin S. A., Andrievsky S. M., Luck R. E., 1999, A&A, 351, 168
Kovtyukh V. V., Soubiran C., Belik S. I., Gorlova N. I., 2003, A&A, 411, 559
Kupka F., Piskunov N. E., Ryabchikova T. A., Stempels H. C., Weiss W. W., 1999, A&AS, 138
Liu N. et al., 2014, ApJ, 786, 66
Martínez-Pinedo G., Fischer T., Huther L., 2014, J. Phys. G Nucl. Phys., 41, 044008
Mashonkina L., Christlieb N., 2014, A&A, 565, A123
Mashonkina L., Gehren T., 2001, A&A, 376, 232
Mashonkina L., Gehren T., Shi J.-R., Korn A. J., Grupp F., 2011, A&A, 528, A87
Matteucci F., Greggio L., 1986, A&A, 154, 279
Matteucci F., Spitoni E., Recchi S., Valiante R., 2009, A&A, 501, 531
Meynet G., Maeder A., 2017, in Supernovae from Rotating Stars, Springer International Publishing AG, Cham, Switzerland, p. 601
Mishenina T. et al., 2015, MNRAS, 446, 3651
Mishenina T. V., Kovtyukh V. V., 2001, A&A, 370, 951
Mishenina T. V., Soubiran C., Kovtyukh V. V., Korotin S. A., 2004, A&A, 418, 551
Mishenina T. V., Soubiran C., Bienaymé O., Korotin S. A., Belik S. I., Usenko I. A., Kovtyukh V. V., 2008, A&A, 489, 923
Mishenina T. V., Pignatari M., Korotin S. A., Soubiran C., Charbonnel C., Thielemann F.-K., Gorbaneva T. I., Basak N. Y., 2013, A&A, 552, A128
Montes F. et al., 2007, ApJ, 671, 1685
Moultaka J., Ilovaisky S. A., Prugniel P., Soubiran C., 2004, PASP, 116, 693
Nishimura N., Takiwaki T., Thielemann F.-K., 2015, ApJ, 810, 109
Nishimura N., Sawai H., Takiwaki T., Yamada S., Thielemann F.-K., 2017, ApJ, 836, L21
Pignatari M., Gallino R., Meynet G., Hirschi R., Herwig F., Wiescher M., 2008, ApJ, 687, L95
Pignatari M., Gallino R., Heil M., Wiescher M., Käppeler F., Herwig F., Bisterzo S., 2010, ApJ, 710, 1557
Pignatari M., Göbel K., Reifarth R., Travaglio C., 2016a, Int. J. Modern Phys. E, 25, 1630003
Pignatari M. et al., 2016b, ApJS, 225, 24
Prantzos N., Abia C., Limongi M., Chieffi A., Cristallo S., 2018, MNRAS, 476, 3432
Qian Y.-Z., Wasserburg G. J., 2001, ApJ, 559, 925
Qian Y.-Z., Wasserburg G. J., 2008, ApJ, 687, 272
Raiteri C. M., Busso M., Picchio G., Gallino R., Pulone L., 1991a, ApJ, 367, 228
Raiteri C. M., Busso M., Picchio G., Gallino R., 1991b, ApJ, 371, 665
Rauscher T., Dauphas N., Dillmann I., Fröhlich C., Fülöp Z., Gyürky G., 2013, Rep. Progr. Phys., 76, 066201
Reddy B. E., Tomkin J., Lambert D. L., Allende Prieto C., 2003, MNRAS, 340, 304
Roberts L. F., Woosley S. E., Hoffman R. D., 2010, ApJ, 722, 954
Roederer I. U., Cowan J. J., Karakas A. I., Kratz K.-L., Lugaro M., Simmerer J., Farouqi K., Sneden C., 2010, ApJ, 724, 975
Roederer I. U., Preston G. W., Thompson I. B., Shectman S. A., Sneden C., Burley G. S., Kelson D. D., 2014, AJ, 147, 136
Roederer I. U., Karakas A. I., Pignatari M., Herwig F., 2016, ApJ, 821, 37
Shchukina N., Trujillo Bueno J., 2001, ApJ, 550, 970
Sneden C., Cowan J. J., Gallino R., 2008, ARA&A, 46, 241
Soubiran C., Bienaymé O., Siebert A., 2003, A&A, 398, 141
Spite M., Spite F., Bonifacio P., Caffau E., François P., Sbordone L., 2014, A&A, 571, A40
Spite F., Spite M., Barbuy B., Bonifacio P., Caffau E., François P., 2018, A&A, 611, A30
Surman R., McLaughlin G. C., Ruffert M., Janka H.-T., Hix W. R., 2008, ApJ, 679, L117
Takahashi K., Witti J., Janka H.-T., 1994, A&A, 286, 857
The L.-S., El Eid M. F., Meyer B. S., 2007, ApJ, 655, 1058
Thévenin F., Idiart T. P., 1999, ApJ, 521, 753
Thielemann F.-K., Eichler M., Panov I. V., Wehmeyer B., 2017, Ann. Rev. Nucl. Particle Sci., 67, 253
Timmes F. X., Woosley S. E., Weaver T. A., 1995, ApJS, 98, 617
Travaglio C., Gallino R., Arnone E., Cowan J., Jordan F., Sneden C., 2004, ApJ, 601, 864
Travaglio C., Hillebrandt W., Reinecke M., 2005, A&A, 443, 1007

Travaglio C., Rauscher T., Heger A., Pignatari M., West C., 2018, ApJ, 854, 18
Trippella O., Busso M., Palmerini S., Maiorca E., Nucci M. C., 2016, ApJ, 818, 125
Tsymbal V., 1996, in Adelman S. J., Kupka F., Weiss W. W., eds, ASP Conf. Ser. Vol. 108, M.A.S.S., Model Atmospheres and Spectrum Synthesis. Astron. Soc. Pac., San Francisco, p. 198
Wanajo S., Janka H.-T., Müller B., 2011a, ApJ, 726, L15
Wanajo S., Janka H.-T., Kubono S., 2011b, ApJ, 729, 46
Wehmeyer B., Pignatari M., Thielemann F.-K., 2015, MNRAS, 452, 1970
Winteler C., Käppeli R., Perego A., Arcones A., Vasset N., Nishimura N., Liebendörfer M., Thielemann F.-K., 2012, ApJ, 750, L22
Woosley S. E., Wilson J. R., Mathews G. J., Hoffman R. D., Meyer B. S., 1994, ApJ, 433, 229
Yong D. et al., 2013, ApJ, 762, 26

APPENDIX

We presented the stellar parameters and the Sr abundances in Table A1.

Table A1. Stellar parameters and abundances of some *n*-capture elements, with the obtained (LTE) Sr abundances, the NLTE corrections from Bergemann et al. (2012), the NLTE Ba and LTE Eu abundance and stellar parameters from Mishenina et al. (2013).

HD/BD	$T_{\rm eff}$, K	log g	[Fe/H]	$V_{\rm t}$	[Sr/Fe]LTE	corr$_{NLTE}$	[Sr/Fe]NLTE	[Ba/Fe]NLTE	[Eu/Fe]
Thin									
166	5514	4.6	0.16	0.6	0.14	0.12	0.16	0.12	− 0.09
1562	5828	4	− 0.32	1.2	0	0.18	0.08	0	
1835	5790	4.5	0.13	1.1	0.27	0.14	0.31	0.04	0.06
3651	5277	4.5	0.15	0.6	0.07	0.11	0.08	− 0.14	− 0.08
4256	5020	4.3	0.08	1.1	0.12	0.11	0.13	− 0.16	
4307	5889	4	− 0.18	1.1	− 0.12	0.17	− 0.04	0.08	0.12
4614	5965	4.4	− 0.24	1.1	− 0.06	0.17	0.01	0.02	0.08
5294	5779	4.1	− 0.17	1.3	0.1	0.17	0.17	0.15	0.01
6660	4759	4.6	0.08	1.4	0.05	0.11	0.06	− 0.15	− 0.03
7590	5962	4.4	− 0.1	1.4	0.08	0.16	0.14	0.11	0.07
7924	5165	4.4	− 0.22	1.1	− 0.13	0.15	− 0.07	− 0.05	0.04
8648	5790	4.2	0.12	1.1	− 0.07	0.14	− 0.02	− 0.04	− 0.13
9407	5666	4.45	0.05	0.8	− 0.07	0.14	− 0.02	− 0.02	− 0.03
9826	6074	4	0.1	1.3	− 0.08	0.15	− 0.02	− 0.02	
10086	5696	4.3	0.13	1.2	− 0.13	0.14	− 0.09	− 0.06	− 0.08
10307	5881	4.3	0.02	1.1	− 0.04	0.15	0.01	− 0.02	0.12
10476	5242	4.3	− 0.05	1.1	0.01	0.14	0.05	0	− 0.06
10780	5407	4.3	0.04	0.9	0.06	0.13	0.09	0.09	0.05
11007	5980	4	− 0.2	1.1	− 0.02	0.17	0.05	0.05	0.19
11373	4783	4.65	0.08	1	0.07	0.11	0.08	− 0.04	− 0.01
12846	5766	4.5	− 0.24	1.2	− 0.08	0.17	0.00	− 0.04	0.16
13507	5714	4.5	− 0.02	1.1	0.07	0.15	0.12	0.11	0.16
14374	5449	4.3	− 0.09	1.1	0.09	0.15	0.14	0.02	0.13
16160	4829	4.6	− 0.16	1.1	− 0.13	0.14	− 0.08	− 0.19	0.28
17674	5909	4	− 0.14	1.1	− 0.12	0.17	− 0.05	− 0.03	− 0.02
17925	5225	4.3	− 0.04	1.1	0.18	0.13	0.21	0.03	0.08
18632	5104	4.4	0.06	1.4	0.04	0.12	0.06	− 0.04	− 0.04
18803	5665	4.55	0.14	0.8	− 0.01	0.13	0.02	0	− 0.02
19019	6063	4	− 0.17	1.1	0.1	0.17	0.17	0.17	
19373	5963	4.2	0.06	1.1	− 0.06	0.15	0.00	− 0.03	0.03
20630	5709	4.5	0.08	1.1	− 0.01	0.14	0.03	0.07	
22049	5084	4.4	− 0.15	1.1	0.03	0.14	0.07	0.15	0.24
22484	6037	4.1	− 0.03	1.1	− 0.07	0.16	− 0.01	0.03	0.02
22556	6155	4.2	− 0.17	1.1	− 0.03	0.17	0.04	0.04	0.21
24053	5723	4.4	0.04	1.1	0.06	0.14	0.10	0.11	0.1
24238	4996	4.3	− 0.46	1	− 0.14	0.18	− 0.05	− 0.12	0.18
24496	5536	4.3	− 0.13	1.5	− 0.12	0.16	− 0.06	− 0.12	0.1
25665	4967	4.7	0.01	1.2	− 0.09	0.12	− 0.06	− 0.03	0.06
25680	5843	4.5	0.05	1.1	− 0.02	0.15	0.03	0.05	0.02
26923	5920	4.4	− 0.03	1	− 0.03	0.16	0.03	0.28	0
28005	5980	4.2	0.23	1.1	0.03	0.14	0.07	0	− 0.13
28447	5639	4	− 0.09	1.1	− 0.11	0.16	− 0.05	0.03	0.13
29150	5733	4.3	0	1.1	− 0.05	0.15	0.00	− 0.03	0.04
29310	5852	4.2	0.08	1.4	− 0.02	0.15	0.03	0.02	
29645	6009	4	0.14	1.3	− 0.11	0.15	− 0.06	− 0.07	− 0.1
30495	5820	4.4	− 0.05	1.3	0.05	0.16	0.11	0.19	0.07
33632	6072	4.3	− 0.24	1.1	− 0.06	0.17	0.01	0.18	0.18
34411	5890	4.2	0.1	1.1	− 0.06	0.15	− 0.01	− 0.01	− 0.01
37008	5016	4.4	− 0.41	0.8	− 0.14	0.17	− 0.06	− 0.24	0.28
37394	5296	4.5	0.09	1.1	0.01	0.12	0.03	0.06	− 0.02
38858	5776	4.3	− 0.23	1.1	− 0.12	0.17	− 0.04	0.03	0.15
39587	5955	4.3	− 0.03	1.5	− 0.05	0.16	0.01	0.14	− 0.03
40616	5881	4	− 0.22	1.1	− 0.13	0.17	− 0.05	0.12	− 0.04

Table A1 – *continued*

HD/BD	$T_{\rm eff}$, K	log g	[Fe/H]	$V_{\rm t}$	[Sr/Fe]LTE	corr$_{NLTE}$	[Sr/Fe]NLTE	[Ba/Fe]NLTE	[Eu/Fe]
41330	5904	4.1	− 0.18	1.2	− 0.12	0.17	− 0.05	0.01	0.22
41593	5312	4.3	− 0.04	1.1	0.09	0.14	0.13	0.1	− 0.07
42618	5787	4.5	− 0.07	1	− 0.08	0.16	− 0.02	0.02	0.09
42807	5719	4.4	− 0.03	1.1	− 0.04	0.15	0.01	0.11	0.05
43587	5927	4.1	− 0.11	1.3	− 0.06	0.16	0.00	− 0.04	0.15
43856	6143	4.1	− 0.19	1.1	− 0.04	0.17	0.03	0.15	0.18
43947	6001	4.3	− 0.24	1.1	− 0.14	0.17	− 0.06	0.06	0.2
45088	4959	4.3	− 0.21	1.2	− 0.32	0.15	− 0.27	0.04	0.13
47752	4613	4.6	− 0.05	0.2	− 0.05	0.13	− 0.02	− 0.02	0.1
48682	5989	4.1	0.05	1.3	− 0.08	0.15	− 0.02	− 0.08	− 0.08
50281	4712	3.9	− 0.2	1.6	0	0.15	0.05	0	
50692	5911	4.5	− 0.1	0.9	− 0.1	0.16	− 0.03	0.03	0.22
51419	5746	4.1	− 0.37	1.1	− 0.13	0.19	− 0.04	− 0.08	0.26
51866	4934	4.4	0	1	0	0.12	0.02	− 0.07	0.02
53927	4860	4.64	− 0.22	1.2	− 0.33	0.15	− 0.28	− 0.02	0.19
54371	5670	4.2	0.06	1.2	0.01	0.14	0.05	− 0.01	0.03
55575	5949	4.3	− 0.31	1.1	− 0.19	0.18	− 0.10	0.02	0.2
58595	5707	4.3	− 0.31	1.2	0.01	0.18	0.09	0.01	0.2
59747	5126	4.4	− 0.04	1.1	0.05	0.13	0.08	0.09	0.02
61606	4956	4.4	− 0.12	1.3	0.02	0.14	0.06	0.02	0.13
62613	5541	4.4	− 0.1	1.1	− 0.05	0.15	0.00	0	− 0.06
63433	5693	4.35	− 0.06	1.9	− 0.09	0.16	− 0.03	0.02	0.03
64468	5014	4.2	0	1.2	0.05	0.12	0.07	− 0.17	
64815	5864	4	− 0.33	1.1	0	0.18	0.08	0.07	0.32
65874	5936	4	0.05	1.3	− 0.05	0.15	0.00	− 0.07	− 0.11
68638	5430	4.4	− 0.24	1.1	− 0.11	0.17	− 0.04	0.05	0.08
70923	5986	4.2	0.06	1.1	− 0.02	0.15	0.03	− 0.06	− 0.12
71148	5850	4.2	0	1.1	− 0.05	0.15	0.00	− 0.01	− 0.06
72760	5349	4.1	0.01	1.1	0.06	0.13	0.09	0.04	0.05
72905	5884	4.4	− 0.07	1.5	− 0.01	0.16	0.05	0.11	0.01
73344	6060	4.1	0.08	1.1	− 0.04	0.15	0.01	− 0.02	− 0.04
73667	4884	4.4	− 0.58	0.9	− 0.2	0.19	− 0.10	− 0.15	0.3
75732	5373	4.3	0.25	1.1	0.01	0.11	0.02	− 0.13	− 0.11
75767	5823	4.2	− 0.01	0.9	− 0.07	0.15	− 0.01	0.04	
76151	5776	4.4	0.05	1.1	− 0.06	0.15	− 0.01	− 0.03	− 0.06
79969	4825	4.4	− 0.05	1	− 0.02	0.13	0.01		0.07
82106	4827	4.1	− 0.11	1.1	0.31	0.13	0.34	0.11	− 0.05
82443	5334	4.4	− 0.03	1.3	0.01	0.14	0.05	0.13	0.12
87883	5015	4.4	0	1.1	− 0.06	0.12	− 0.03	− 0.05	0.02
88072	5778	4.3	0	1.1	− 0.04	0.15	0.01	− 0.03	0.15
89251	5886	4	− 0.12	1.1	− 0.08	0.16	− 0.01	0.05	0.16
89269	5674	4.4	− 0.23	1.1	− 0.07	0.17	0.00	0.03	0.2
91347	5931	4.4	− 0.43	1.1	− 0.15	0.19	− 0.05	− 0.02	0.22
94765	5077	4.4	− 0.01	1.1	0.09	0.13	0.12	0.07	
95128	5887	4.3	0.01	1.1	− 0.08	0.15	− 0.02	− 0.05	0
97334	5869	4.4	0.06	1.2	− 0.05	0.15	0.00	0.13	− 0.01
97658	5136	4.5	− 0.32	1.2	− 0.18	0.16	− 0.11	− 0.03	0.19
98630	6060	4	0.22	1.4	− 0.14	0.14	− 0.09	− 0.09	− 0.1
101177	5932	4.1	− 0.16	1.1	− 0.06	0.17	0.01	0.01	0.15
102870	6055	4	0.13	1.4	− 0.11	0.15	− 0.06	− 0.03	− 0.09
105631	5416	4.4	0.16	1.2	− 0.08	0.12	− 0.05	− 0.02	− 0.04
107705	6040	4.2	0.06	1.4	− 0.11	0.15	− 0.05	0.06	− 0.05
108954	6037	4.4	− 0.12	1.1	− 0.05	0.17	0.02	0.11	0.06
109358	5897	4.2	− 0.18	1.1	− 0.13	0.17	− 0.06	− 0.05	0.04
110463	4950	4.5	− 0.05	1.2	0	0.13	0.03	0.04	0.09
110833	5075	4.3	0	1.1	0.04	0.12	0.06	− 0.04	
111395	5648	4.6	0.1	0.9	0.02	0.14	0.02	0.19	0.02
112758	5203	4.2	− 0.56	1.1	0.17	0.19	− 0.07	− 0.22	
114710	5954	4.3	0.07	1.1	0.05	0.15	0.00	0.11	− 0.03

Table A1 *– continued*

HD/BD	$T_{\rm eff}$, K	log g	[Fe/H]	$V_{\rm t}$	[Sr/Fe]LTE	corr$_{NLTE}$	[Sr/Fe]NLTE	[Ba/Fe]NLTE	[Eu/Fe]
115383	6012	4.3	0.11	1.1	0.03	0.15	0.02	0.12	0.05
115675	4745	4.45	0.02	1	0.02	0.12	0.00	− 0.07	0.03
116443	4976	3.9	− 0.48	1.1	0.14	0.18	− 0.05	− 0.18	0.17
116956	5386	4.55	0.08	1.2	0.03	0.13	0.00	0.05	0.04
117043	5610	4.5	0.21	0.4	0.04	0.13	0.07	0.1	− 0.07
119802	4763	4	− 0.05	1.1	0.23	0.13	0.26	0.02	− 0.06
122064	4937	4.5	0.07	1.1	0.03	0.11	0.04	− 0.07	0.07
124642	4722	4.65	0.02	1.3	− 0.03	0.12	− 0.01	− 0.02	0.1
125184	5695	4.3	0.31	0.7	− 0.03	0.12	− 0.01	0.04	− 0.07
126053	5728	4.2	− 0.32	1.1	− 0.14	0.18	− 0.06	− 0.13	0.06
127506	4542	4.6	− 0.08	1.2	− 0.27	0.14	− 0.23	− 0.04	0.08
128311	4960	4.4	0.03	1.3	0.03	0.12	0.05	− 0.03	0.04
130307	4990	4.3	− 0.25	1.4	− 0.15	0.16	− 0.09	0.08	0.2
130948	5943	4.4	− 0.05	1.3	− 0.03	0.16	0.03	0.15	0.07
131977	4683	3.7	− 0.24	1.8	0.09	0.15	0.14	− 0.11	0.18
135599	5257	4.3	− 0.12	1	0.04	0.15	0.09	0.1	0.11
137107	6037	4.3	0	1.1	0.01	0.16	0.07	0.09	
139777	5771	4.4	0.01	1.3	− 0.03	0.15	0.02	0.14	− 0.09
139813	5408	4.5	0	1.2	− 0.02	0.14	0.02	0.15	0.12
140538	5675	4.5	0.02	0.9	0.02	0.15	0.07	0.06	0.12
141004	5884	4.1	− 0.02	1.1	− 0.08	0.16	− 0.02	0	0.11
141272	5311	4.4	− 0.06	1.3	− 0.09	0.14	− 0.04	0.14	0.08
142267	5856	4.5	− 0.37	1.1	− 0.15	0.19	− 0.06	− 0.03	0.19
144287	5414	4.5	− 0.15	1.1	− 0.11	0.15	− 0.05	− 0.03	
145675	5406	4.5	0.32	1.1	− 0.02	0.10	− 0.01	− 0.09	− 0.03
146233	5799	4.4	0.01	1.1	− 0.02	0.15	0.03	0.01	0.08
149661	5294	4.5	− 0.04	1.1	0.02	0.14	0.06	0.01	0.03
149806	5352	4.55	0.25	0.4	0.05	0.11	0.06	0.05	− 0.08
151541	5368	4.2	− 0.22	1.3	− 0.15	0.16	− 0.08	− 0.15	0.26
153525	4810	4.7	− 0.04	1	− 0.11	0.13	− 0.08	0.04	0.16
154345	5503	4.3	− 0.21	1.3	− 0.1	0.17	− 0.03	− 0.05	0.15
156668	4850	4.2	− 0.07	1.2	− 0.13	0.13	− 0.09	− 0.13	0.05
156985	4790	4.6	− 0.18	1	− 0.1	0.14	− 0.05	− 0.09	0.2
158633	5290	4.2	− 0.49	1.3	− 0.19	0.19	− 0.09	− 0.16	0.08
160346	4983	4.3	− 0.1	1.1	0.05	0.14	0.09	− 0.08	0.04
161098	5617	4.3	− 0.27	1.1	− 0.11	0.17	− 0.03	− 0.02	0.26
164922	5392	4.3	0.04	1.1	− 0.01	0.13	0.02	− 0.1	0.1
165173	5505	4.3	− 0.05	1.1	− 0.12	0.15	− 0.07	− 0.07	0.09
165341	5314	4.3	− 0.08	1.1	− 0.02	0.14	0.02	0.03	0
165476	5845	4.1	− 0.06	1.1	− 0.12	0.16	− 0.05	− 0.06	
165670	6178	4	− 0.1	1.5	− 0.1	0.16	− 0.03	0.1	
165908	5925	4.1	− 0.6	1.1	− 0.15	0.20	− 0.04	0.04	0.14
166620	5035	4	− 0.22	1	− 0.08	0.15	− 0.02	− 0.09	0.16
171314	4608	4.65	0.07	1	− 0.02	0.12	0.00	− 0.09	0.1
174080	4764	4.55	0.04	1	0.09	0.12	0.11	− 0.01	0.13
176377	5901	4.4	− 0.17	1.3	− 0.08	0.17	− 0.01	0.05	0.14
176841	5841	4.3	0.23	1.1	− 0.08	0.13	− 0.04	− 0.12	− 0.09
178428	5695	4.4	0.14	1	− 0.07	0.14	− 0.03	0.04	0.03
180161	5473	4.5	0.18	1.1	0.02	0.12	0.04	0.07	− 0.01
182488	5435	4.4	0.07	1.1	− 0.03	0.13	0.00	− 0.07	− 0.03
183341	5911	4.3	− 0.01	1.3	− 0.1	0.16	− 0.04	− 0.08	0.1
184385	5536	4.45	0.12	0.9	0	0.13	0.03	0.07	− 0.02
185144	5271	4.2	− 0.33	1.1	− 0.03	0.17	0.04	− 0.02	0.17
185414	5818	4.3	− 0.04	1.1	− 0.11	0.16	− 0.05	0.07	0.04
186408	5803	4.2	0.09	1.1	− 0.04	0.15	0.01	− 0.03	− 0.05
186427	5752	4.2	0.02	1.1	− 0.08	0.15	− 0.03	− 0.07	0.02
187897	5887	4.3	0.08	1.1	− 0.03	0.15	0.02	0.03	
189087	5341	4.4	− 0.12	1.1	− 0.03	0.15	0.02	0.1	0.06
189733	5076	4.4	− 0.03	1.5	− 0.09	0.13	− 0.06	− 0.11	0.05

Table A1 – *continued*

HD/BD	$T_{\rm eff}$, K	log g	[Fe/H]	$V_{\rm t}$	[Sr/Fe]LTE	corr$_{NLTE}$	[Sr/Fe]NLTE	[Ba/Fe]NLTE	[Eu/Fe]
190007	4724	4.5	0.16	0.8	0.12	0.10	0.12	− 0.03	− 0.04
190406	5905	4.3	0.05	1	− 0.06	0.15	− 0.01	0.05	− 0.03
190470	5130	4.3	0.11	1	0	0.11	0.01	− 0.08	0.01
190771	5766	4.3	0.13	1.5	− 0.12	0.14	− 0.08	− 0.07	− 0.06
191533	6167	3.8	− 0.1	1.5	− 0.02	0.16	0.04	0.09	− 0.06
191785	5205	4.2	− 0.12	1.2	− 0.15	0.14	− 0.10	− 0.24	0.14
195005	6075	4.2	− 0.06	1.3	0.01	0.16	0.07	0.06	
195104	6103	4.3	− 0.19	1.1	− 0.01	0.17	0.06	0.2	0.03
197076	5821	4.3	− 0.17	1.2	0.02	0.17	0.09	0.08	0.21
199960	5878	4.2	0.23	1.1	− 0.13	0.14	− 0.09	− 0.11	
200560	5039	4.4	0.06	1.1	0.09	0.12	0.11	0.04	− 0.09
202108	5712	4.2	− 0.21	1.1	− 0.04	0.17	0.03	0.1	0.15
202575	4667	4.6	− 0.03	0.5	− 0.02	0.13	0.01	0.09	0.1
203235	6071	4.1	0.05	1.3	− 0.08	0.16	− 0.02	− 0.05	− 0.01
205702	6020	4.2	0.01	1.1	− 0.03	0.16	0.03	− 0.03	− 0.02
206860	5927	4.6	− 0.07	1.8	− 0.08	0.16	− 0.01	0.05	
208038	4982	4.4	− 0.08	1	0.13	0.13	0.16	0.09	0.1
208313	5055	4.3	− 0.05	1	− 0.09	0.13	− 0.05	− 0.09	− 0.03
208906	5965	4.2	− 0.8	1.7	− 0.05	0.22	0.07	− 0.14	0.34
210667	5461	4.5	0.15	0.9	0.05	0.12	0.07	− 0.04	− 0.01
210752	6014	4.6	− 0.53	1.1	− 0.1	0.2	0.00	0.03	0.37
211472	5319	4.4	− 0.04	1.1	0.02	0.14	0.06	0.1	
214683	4747	4.6	− 0.46	1.2	− 0.09	0.18	− 0.01	0.06	0.28
216259	4833	4.6	− 0.55	0.5	− 0.2	0.19	− 0.11	− 0.1	0.22
216520	5119	4.4	− 0.17	1.4	− 0.28	0.15	− 0.23	− 0.2	0.09
217014	5763	4.3	0.17	1.1	− 0.05	0.14	− 0.01	− 0.1	− 0.05
217813	5845	4.3	0.03	1.5	− 0.05	0.15	0.00	0.04	− 0.01
218868	5547	4.45	0.21	0.4	0.19	0.12	0.21	0.03	− 0.03
219538	5078	4.5	− 0.04	1.1	− 0.08	0.13	− 0.04	− 0.06	0.06
219623	5949	4.2	0.04	1.2	− 0.09	0.15	− 0.03	0.01	0.13
220182	5364	4.5	− 0.03	1.2	− 0.02	0.14	0.02	0.07	0.1
220221	4868	4.5	0.16	0.5	0.24	0.10	0.24	0.02	− 0.09
221851	5184	4.4	− 0.09	1	− 0.08	0.14	− 0.03	0.02	0.11
222143	5823	4.45	0.15	1.1	− 0.1	0.14	− 0.05	0.09	− 0.02
224465	5745	4.5	0.08	0.8	− 0.04	0.14	0.00	0.05	0.04
263175	4734	4.5	− 0.16	0.5	− 0.06	0.14	− 0.02	− 0.13	0.23
BD12063	4859	4.4	− 0.22	0.6	0.02	0.15	0.07	0.07	0.05
BD124499	4678	4.7	0	0.5	0.04	0.12	0.06	0.02	0.24
Thick disc									
245	5400	3.4	− 0.84	0.7	− 0.06	0.23	0.07	0.02	0.35
3765	5079	4.3	0.01	1.1	0.09	0.12	0.11	− 0.09	0.03
5351	4378	4.6	− 0.21	0.5	–	0.16	–	− 0.33	0.08
6582	5240	4.3	− 0.94	0.7	− 0.02	0.24	0.12	− 0.12	0.41
13783	5350	4.1	− 0.75	1.1	− 0.05	0.22	0.07	− 0.08	0.39
18757	5741	4.3	− 0.25	1	− 0.1	0.17	− 0.02	− 0.08	0.22
22879	5972	4.5	− 0.77	1.1	0.03	0.22	0.15	0.05	0.41
65583	5373	4.6	− 0.67	0.7	0.07	0.21	0.18	− 0.07	0.41
76932	5840	4	− 0.95	1	0.1	0.23	0.23	0.1	
106516	6165	4.4	− 0.72	1.1	− 0.13	0.20	− 0.02	0.09	
110897	5925	4.2	− 0.45	1.1	− 0.12	0.19	− 0.02	− 0.01	0.29
135204	5413	4	− 0.16	1.1	0.01	0.15	0.06	− 0.11	0.2
152391	5495	4.3	− 0.08	1.3	0.03	0.15	0.08	0.03	0.12
157089	5785	4	− 0.56	1	− 0.06	0.20	0.04	0.02	0.37
157214	5820	4.5	− 0.29	1	− 0.06	0.18	0.02	− 0.05	0.21
159062	5414	4.3	− 0.4	1	0.2	0.18	0.28	0.15	0.29
165401	5877	4.3	− 0.36	1.1	− 0.12	0.18	− 0.02	− 0.12	0.27
190360	5606	4.4	0.12	1.1	− 0.05	0.13	− 0.01	− 0.06	0.02
201889	5600	4.1	− 0.85	1.2	0.05	0.23	0.18	0.01	0.34
201891	5850	4.4	− 0.96	1	− 0.1	0.24	0.04	− 0.06	

Table A1 *– continued*

HD/BD	$T_{\rm eff}$, K	log g	[Fe/H]	$V_{\rm t}$	[Sr/Fe]LTE	corr$_{NLTE}$	[Sr/Fe]NLTE	[Ba/Fe]NLTE	[Eu/Fe]
204521	5809	4.6	– 0.66	1.1	– 0.06	0.21	0.05	– 0.06	0.3
Hercules stream									
13403	5724	4	– 0.31	1.1	– 0.06	0.18	0.02	– 0.09	0.15
19308	5844	4.3	0.08	1.1	– 0.08	0.15	– 0.03	– 0.01	– 0.04
23050	5929	4.4	– 0.36	1.1	– 0.08	0.18	0.00	– 0.04	0.25
30562	5859	4	0.18	1.1	– 0.08	0.14	– 0.03	0.02	0.02
64606	5250	4.2	– 0.91	0.8	0.03	0.24	0.17	– 0.14	0.4
68017	5651	4.2	– 0.42	1.1	– 0.1	0.19	– 0.01	– 0.12	0.26
81809	5782	4	– 0.28	1.3	– 0.12	0.18	– 0.04	– 0.15	0.17
107213	6156	4.1	0.07	1.6	– 0.07	0.15	– 0.01	0.02	
139323	5204	4.6	0.19	0.7	0.31	0.11	0.32	0.00	0.1
139341	5242	4.6	0.21	0.9	– 0.06	0.10	– 0.05	– 0.07	0.13
144579	5294	4.1	– 0.7	1.3	0	0.21	0.11	– 0.25	0.24
159222	5834	4.3	0.06	1.2	– 0.09	0.15	– 0.03	– 0.03	– 0.07
159909	5749	4.1	0.06	1.1	– 0.13	0.14	– 0.08	– 0.11	– 0.03
215704	5418	4.2	0.07	1.1	– 0.03	0.13	0.00	– 0.12	– 0.03
218209	5705	4.5	– 0.43	1	– 0.08	0.19	0.01	– 0.01	– 0.03
221354	5242	4.1	– 0.06	1.2	– 0.12	0.14	– 0.07	– 0.26	– 0.03
Non-classified									
4628	4905	4.6	– 0.36	0.5	– 0.09	0.16	– 0.02	– 0.04	
4635	5103	4.4	0.07	0.8	0.03	0.12	0.05	– 0.04	0
10145	5673	4.4	– 0.01	1.1	– 0.11	0.15	– 0.05	– 0.06	0.15
12051	5458	4.55	0.24	0.5	– 0.04	0.11	– 0.02	0.1	– 0.07
13974	5590	3.8	– 0.49	1.1	– 0.11	0.19	– 0.01	– 0.01	0.01
17660	4713	4.75	0.17	1.3	0.03	0.10	0.03	– 0.14	0.15
20165	5145	4.4	– 0.08	1.1	– 0.02	0.14	0.02	– 0.07	0
24206	5633	4.5	– 0.08	1.1	– 0.04	0.15	0.018	0.03	0.07
32147	4945	4.4	0.13	1.1	0.27	0.11	0.28	– 0.04	0.06
45067	6058	4	– 0.02	1.2	– 0.1	0.16	– 0.03	0	– 0.04
84035	4808	4.8	0.25	0.5	0.11	0.09	0.10	– 0.05	– 0.08
86728	5725	4.3	0.22	0.9	– 0.07	0.13	– 0.03	– 0.06	– 0.1
90875	4788	4.5	0.24	0.5	0.26	0.09	0.25	– 0.01	
117176	5611	4	– 0.03	1	– 0.07	0.15	– 0.01	– 0.01	0.07
117635	5230	4.3	– 0.46	0.7	– 0.02	0.18	0.06	– 0.04	0.3
154931	5910	4	– 0.1	1.1	– 0.09	0.16	– 0.02	0.01	– 0.01
159482	5620	4.1	– 0.89	1	– 0.03	0.23	0.10	– 0.01	0.35
168009	5826	4.1	– 0.01	1.1	– 0.09	0.15	– 0.03	– 0.06	0.05
173701	5423	4.4	0.18	1.1	– 0.01	0.12	0.01	– 0.1	– 0.14
182736	5430	3.7	– 0.06	1	0.03	0.14	0.07	0.05	
184499	5750	4	– 0.64	1.5	– 0.04	0.21	0.07	– 0.1	0.37
184768	5713	4.2	– 0.07	1.1	– 0.09	0.15	– 0.03	– 0.09	0.11
186104	5753	4.2	0.05	1.1	– 0.07	0.15	– 0.02	– 0.05	0.09
215065	5726	4	– 0.43	1.1	– 0.15	0.19	– 0.05	– 0.16	
219134	4900	4.2	0.05	0.8	0.05	0.11	0.06	– 0.03	– 0.11
219396	5733	4	– 0.1	1.2	– 0.1	0.16	– 0.03	– 0.09	
224930	5300	4.1	– 0.91	0.7	– 0.04	0.24	0.10	– 0.09	

This paper has been typeset from a TEX/LATEX file prepared by the author.